[redacted]

Copy 5
RM L56C07

C.1

NACA

RESEARCH MEMORANDUM

AN EXPERIMENTAL INVESTIGATION OF THE EFFECTS OF SEVERAL DIFFUSERS AND DIFFUSER-ENTRANCE—MIXING-SECTION COMBINATIONS ON THE POWER REQUIREMENTS OF A $4\frac{1}{2}$ - INCH BY $4\frac{1}{2}$ - INCH SLOTTED TRANSONIC WIND TUNNEL

By John S. Dennard

Langley Aeronautical Laboratory
Langley Field, Va.

NATIONAL ADVISORY COMMITTEE
FOR AERONAUTICS

WASHINGTON
June 5, 1956

[redacted]

NACA RM L56C07

NATIONAL ADVISORY COMMITTEE FOR AERONAUTICS

RESEARCH MEMORANDUM

AN EXPERIMENTAL INVESTIGATION OF THE EFFECTS OF SEVERAL DIFFUSERS AND DIFFUSER-ENTRANCE—MIXING-SECTION COMBINATIONS ON THE POWER REQUIREMENTS OF A $4\frac{1}{2}$-INCH BY $4\frac{1}{2}$-INCH SLOTTED TRANSONIC WIND TUNNEL

By John S. Dennard

SUMMARY

A $4\frac{1}{2}$-inch by $4\frac{1}{2}$-inch tunnel in which two opposite walls were slotted has been tested to determine the effects of various slot exit shapes, mixing sections, and diffusers on power requirements. Information obtained included measurements of the overall pressure ratio required to operate the tunnel, the effects of auxiliary bleed flow, diffuser static-pressure ratios and distributions, and diffuser total pressure distributions. Power parameters were determined from the integrated values of the total pressures at the diffuser exit together with the auxiliary bleed-flow rate.

The maximum test Mach number of the transonic tunnel without auxiliary bleed flow is dependent upon the geometry of the air passages downstream of the slotted portions of the test section and is limited by choking. The maximum test Mach number is increased as bleed flow is increased through auxiliary pumping. Maximum Mach numbers were obtained most efficiently through a combination of auxiliary pumping and ejector pumping.

A long diffuser with a gradual curve at the entrance provided higher Mach numbers than a shorter, straight-wall diffuser which had an abrupt change of shape at the entrance; however, a short, smaller area-ratio diffuser with a gradual curve at the entrance required, as expected, less power than any other configuration tested. This low power is attained by the elimination of losses in the downstream regions of the diffuser at the expense of higher diffuser exit velocities. The addition of shrouds covering the downstream ends of the slots or the boattailing of bars between adjacent slots gave only small changes in the attainable Mach number. Contraction in the mixing section was found to cause choking and increase the auxiliary bleed-flow requirements and to induce large regions of supersonic flow at the diffuser entrance with attendant increases in main-stream power.

INTRODUCTION

An investigation conducted in the Langley 8-foot transonic tunnel (ref. 1) has pointed out that a large portion of the power losses associated with slotted tunnels are concentrated in the reentry region where the low-energy plenum air, which had been expanded through the slots, rejoins the main stream. Tests made in a small-scale single-slot test section (ref. 2) showed that power requirements were effected by modification of the slot and tunnel geometry in this region of the tunnel which is referred to herein as the "ejector." The tests of reference 2 also indicated that, up to $M = 1.2$, a tunnel in which all low-energy slot-flow air is removed by an auxiliary pump reguired less power than one which used an ejector. The Mach number attained with a combination of ejector pumping and auxiliary pumping together with variable-angle reentry flaps was reported in references 3 and 4.

The present investigation has been conducted to explore further the combination of auxiliary pumping with a variety of ejectors to remove the low-energy air from the chamber surrounding the test section and thus increase the Mach number attainable and/or reduce the power requirements of the system. Several ejector and diffuser configurations have been investigated to determine their influence on the overall power requirements. The diffusers were all two dimensional and the diverging walls were primarily straight-line sections with, in some instances, a faired approach in the upstream sections. Tests were conducted where the two diverging diffuser walls were in one case continuations of the two slotted test-section walls and in the other case were continuations of the two solid test-section walls.

The data presented herein include total-pressure measurements of the secondary flow at the ejector exit, and total and static pressure distributions at the diffuser exits. The data were obtained at Reynolds numbers from 4×10^6 to 7×10^6 per foot. The flaps and ejector configurations of the tunnel used in the present investigation and in that of reference 4 are comparable, but the diffusers of reference 4 were all circular and had transition sections to match the square tunnel to the circular diffuser. The larger test-section size, together with the much higher stagnation pressures used in reference 4, provides a ratio of Reynolds number of 4:1 between reference 4 and the present investigation.

SYMBOLS

C a factor in the power parameter, $\frac{m_o J g c_p}{550} = 10.97 m_o$

c_p specific heat of air at constant pressure, 0.241 Btu/lb/°F

g gravitational constant, 32.174 ft/sec^2

P power parameter, (Bleed flow power + Main stream power),

$$CT_o\left[\frac{m_b}{m_o}\left(\frac{\gamma - 1}{2}\right)M^2\right] + CT_o\left(1 - \frac{m_b}{m_o}\right)\left[\left(\frac{H_o}{H_e}\right)^{\frac{\gamma-1}{\gamma}} - 1\right], \text{ horsepower}$$

H total pressure, lb/sq ft

J mechanical equivalent of heat, 778 ft-lb/Btu

m mass flow, slugs/sec

M Mach number, based on p_c/H_o

p static pressure, lb/sq ft

T temperature, ^oR

X diffuser station measured in direction of flow, in.

Y ordinate, measured vertically from center line

Z ordinate, measured horizontally from center line

γ ratio of specific heats

δ_F flap angle (see fig. 3(c))

Subscripts:

b bleed flow (handled by auxiliary pump)

c plenum chamber

e diffuser exit

o free stream at entrance to test section

APPARATUS AND METHODS

Test Apparatus

The general arrangement of the test setup is shown in the sketch of figure 1. The test-section walls, with exceptions in the boattailed region, are identical to those of reference 3. Air at total pressures

[redacted]

up to 2 atmospheres is supplied from a 1000-horsepower compressor, accelerated to sonic velocity through an entrance bell of conventional design, and enters the model slotted test section where further acceleration of the main stream is accomplished by removing part of the air from the test section through the slotted boundary. This slot-flow air, having lost a large part of its energy in the slots, is then withdrawn from the circuit by a vacuum pump connected to the plenum chamber, as in reference 3, or returned to the main stream through an ejector and hence discharged to the atmosphere through a subsonic diffuser. The air removed by the vacuum pump is discharged through a 6-inch line equipped with a calibrated orifice and a butterfly valve for auxiliary bleed-flow control.

An arrangement whereby all slot-flow air is removed from the plenum chamber by auxiliary pumping is shown in figure 2. Various ejector arrangements are shown in the line drawings of figure 3. The cross section at which the flow over the flaps exhausts into the mixing section is defined as the ejector. (See fig. 3(a).) For its operation, the ejector depends on entrainment of the induced (ejected) slot flow by the main tunnel air stream. Several variations of conventional ejector arrangements, such as those shown in figures 3(a) and 3(b) where a shroud (solid plate) separates the main stream (primary jet) from the slot flow (secondary jet), were tested. For these configurations, the mixing-section area distribution was varied but the ejector gap was fixed at 1/2 inch which is comparable to configuration II of reference 3. Other ejector configurations included a variety of "open" ejectors where the slots were continued uninterrupted to the mixing tube as shown in figure 3(c). Adjustable flaps were located within the slots to direct the slot-flow air into the mixing tube as shown in figure 3.

Five different diffusers were used in the course of the investigation; each diffuser is identified by a Roman numeral and the ordinates are given in table I. Since the area increase afforded by the ejector contributes directly to the overall stream diffusion, the diffuser area ratio, as listed, includes the total area expansion from test section to diffuser exit. The diffuser equivalent conical angle is defined by considering only the section from the mixing-section exit to the diffuser exit; consequently, the equivalent conical angles reported herein are calculated only for the sections beginning at station 0. (See fig. 3(b).) The included angle between the straight-line portions of the diverging walls (wall divergence angle) is also included for convenience of comparison. Diffuser I has an area ratio of 2:1 with parallel side walls and straight-line upper and lower walls diverging at an effective conical angle of 5.76°. This diffuser had an abrupt break at the mixing-section—diffuser juncture with no attempt made to fair the diffuser entrance. All other diffusers were made up of both curved and straight-line elements. The arrows in table I represent a straight-line variation except where noted. Equivalent conical angles downstream of the mixing section were 3.59° for diffusers II and III, 1.55° for diffuser IV,

and 3.06° for diffuser V. Cross-sectional areas for the different diffusers and mixing-section contractions are given in figure 4.

Instrumentation

Total pressure H_o was measured in the duct slightly upstream of the entrance bell. Static-pressure orifices were installed in the plenums and in longitudinal rows in the diffuser; one row was centered along the center line of one side wall and the other row along the center line of the bottom wall of all the curved-wall diffusers. The straight-wall diffuser had only one row of orifices along a side wall. A rake consisting of total- and static-pressure tubes was provided at the diffuser exit and a total-pressure tube was centered in each of four slots at the end of the slotted section. A static-pressure orifice was located near the tunnel throat for measurement of total mass flow. Two static-pressure orifices for the calibrated bleed-flow orifice completed the instrumentation. All pressures were photographically recorded from a multiple-tube manometer.

Test Procedure and Data Reduction

For tests without auxiliary pumping, the flap angle δ_F was set and the Mach number was varied by changing the total pressure. For tests where auxiliary pumping was used, the flap angle and total pressure were maintained constant and Mach number changes accomplished by varying the bleed flow. This procedure was repeated for several values of the total pressure at three flap angles.

The test-section Mach number was computed from the plenum-chamber static pressure p_c and the total pressure H_o. The overall pressure ratio H_o/p_e, much used herein as a basic performance parameter, is the ratio of the upstream total pressure H_o to the diffuser-exit static pressure p_e which is approximately equal to atmospheric pressure. Power parameters were calculated by assuming adiabatic compression of the main stream from the measured diffuser-exit total pressure and of the bleed flow from the plenum-chamber static pressure to H_o. This is expressed in the following equation:

$$P = \frac{m_o g J c_p}{550} T_o \left\{ \underbrace{\frac{m_b}{m_o}\left[\left(\frac{H_o}{p_c}\right)^{\frac{\gamma-1}{\gamma}} - 1\right]}_{\text{Bleed flow}} + \underbrace{\left(1 - \frac{m_b}{m_o}\right)\left[\left(\frac{H_o}{H_e}\right)^{\frac{\gamma-1}{\gamma}} - 1\right]}_{\text{Main stream}} \right\}$$

[redacted]

The bleed-flow term is further simplified by converting it to a Mach number expression. The final form of the equation is then

$$\frac{P}{CT_o} = \frac{m_b}{m_o}\left(\frac{\gamma - 1}{2}\right)M^2 + \left(1 - \frac{m_b}{m_o}\right)\left[\left(\frac{H_o}{H_e}\right)^{\frac{\gamma-1}{\gamma}} - 1\right]$$

RESULTS AND DISCUSSION

Performance

Tests of the various configurations of this $4\frac{1}{2}$-inch-square slotted tunnel have provided the results presented in figures 5 to 9. For these figures, data are presented only for $\delta_F = 10^\circ$ since this flap angle appeared to be near an optimum for generation of high Mach number at low tunnel pressure ratios, H/p_e (ref. 3).

Effects of tunnel pressure ratio and bleed-flow rate on Mach number.- Figure 5 shows the test section Mach number as a function of tunnel pressure ratio for constant bleed-flow rates. The initial rise in M is very rapid at low values of H_o/p_e but, at the higher values of tunnel pressure ratio, the Mach number increase is more gradual and, in most cases, tends to become constant. For every value of the tunnel pressure ratio, increasing the bleed-flow rate (by auxiliary pumping) always results in increases in Mach number. A dotted line shown on each set of curves indicates the theoretical one-dimensional variation of Mach number with bleed-flow rate. To the left of or below this line, the Mach number attained is less than that corresponding to one-dimensional flow; for those configurations which incorporate an ejector, this suggests possible reversal of flow through the ejector and into the chamber surrounding the tunnel, and for the nonejector configuration, figure 5(g), indicates excessive flow into this chamber through the downstream region of the slots. Points above or to the right of the dotted line indicate Mach numbers in excess of those which correspond to the auxiliary air removal rate, hence, indicate that part of the slot-flow air was being handled through the ejector. As the tunnel pressure ratio is increased, the ejector begins to pump a very sizeable proportion of the flow, amounting to about 12 percent of the total flow, based on one-dimensional considerations, at $M = 1.54$ and $H_o/p_e = 1.92$ for the boattailed slots and diffuser III, figure 5(h).

For the specific configurations, the curves of figure 5 may be used to a large extent for performance comparisons. These figures are grouped for ease of comparison according to diffuser configurations; thus the data of figures 5(a) to 5(e) were taken with diffusers I and II in which

the divergence was restricted to planes normal to the slotted walls; that of figures 5(f) to 5(i) were taken with diffuser III, a 3.59° diffuser in which the wall divergence was in planes parallel to the slotted walls; and for figures 5(j) and (k), diffusers IV and V, the area ratio was reduced to approximately 1.5.

Figures 5(a), (b), and (c) are all for long shrouds and diffuser I, but with varying convergence in the mixing section. It is seen that, generally, the convergence of the mixing section has reduced the Mach number attained for any given combination of tunnel pressure ratio and bleed-flow rate as a result of reduced ejector effectiveness.

A comparison of the data for long and short shrouds using diffuser I (figs. 5(a) and (d)) and a constant-area mixing section at very low tunnel pressure ratios $H_o/p_e = 1.125$ shows higher Mach numbers at high bleed-flow rates with the long shroud, but for the higher tunnel pressure ratios, differences between the two configurations are negligible.

Figures 5(d), (e), and (f) offer a comparison of the performance of the short-shroud configuration with constant-area mixing and three different diffusers. For these three diffusers, the highest Mach number is provided by diffuser III throughout the test range. This is the diffuser for which the expansion occurs downstream of the solid tunnel walls; the only divergence downstream of the slotted walls is that which is afforded by the ejector.

Results of tests using the sharp-slot cutoff are presented in figure 5(g). For this configuration (see fig. 2), it is noted that the curves are nearly flat for the higher pressure ratios and that the knee is much more abrupt than those for the configurations using ejector pumping with $\delta_F = 10°$. This abrupt knee and flattening at high tunnel pressure ratios, however, was also observed in the unpublished data for the ejector configurations when operated at $\delta_F = 0°$. These curves indicate clearly the effect of the lack of ejector pumping on the attainable Mach number.

A comparison of the data for the closed ejectors (short shrouds) and the open ejectors (boattailed slots with and without the flat tops on the bars (see fig. 3(c)) using diffuser III may be obtained from figures 5(f), 5(h), and 5(i). There is a definite, although small, improvement throughout the test range in the Mach number attained with the open-ejector configurations.

The effects of diffuser area ratio and conical angle on the opened-boattail configuration may be seen in figures 5(i), 5(j), and 5(k). It is seen that diffusers IV and V provide maximum Mach numbers in the same range as diffuser III; however, the Mach number performance is impaired

at the lower values of tunnel pressure ratios by use of the smaller area ratio diffusers.

Effects of tunnel pressure ratio and bleed-flow rate on diffuser static pressure.- Curves showing the ratio of the diffuser-exit static pressure to that in the chamber surrounding the test section are presented in figure 6 as a function of tunnel pressure ratio for constant auxiliary bleed-flow rates. These curves, which are exactly calculable from the curves of figure 5, are characterized by a peak diffuser static pressure ratio which occurs at a tunnel pressure ratio corresponding to the knee of the curves of Mach number as a function of tunnel pressure ratio of figure 5. The diffuser static pressure rise drops sharply for both larger and smaller values of H_o/p_e. The effect of bleed-flow rate on the diffuser static pressure rise is very strong, the reason being the reduction of plenum static pressure as the Mach number is increased by auxiliary bleed while the exit static pressure remains essentially constant.

The static pressure ratio is determined by the stream Mach number and the tunnel pressure ratio; consequently, lines of constant Mach number may be superimposed on these data. This was done in figure 6(h) where curves for the boattailed bars and diffuser III, one of the better configurations investigated in this program, are presented. Along these curves of constant Mach number, the value of p_e/p_c decreases steadily as H_o/p_e increases. The experimental curves follow the general trend of the constant Mach number curves at the higher values of H_o/p_e as was observed in figure 5. At low values of H_o/p_e, the rapid increase in static pressure ratio is consistent with increases in Mach number and H_o/p_e.

The variation of static pressure along the walls of the mixing section and diffuser is presented in figure 7. At the entrance to the mixing section the static pressure, in general, approaches that of the plenum chamber. Since the diffuser exit is subsonic, all curves for a given H_o/p_e will be nearly identical in the downstream portions of the diffuser and the end point for each curve is necessarily the reciprocal of the tunnel pressure ratio. At the lower tunnel pressure ratios, the static pressure increased continuously through the mixing section and the diffuser, but at the higher values of H_o/p_e, regions of decreasing pressure often appear in the mixing section and near the diffuser entrance, indicating an expansion (acceleration) before the compression.

A comparison of figures 7(a), (b), and (c) at $m_b/m_o = 0$, to isolate auxiliary pumping effects, offers an explanation for the reduction in peak Mach numbers observed when using the converging blocks in the mixing section. Use of convergence reduces the overall flow area in the mixing

section and consequently forces the ejected bleed air to flow through a comparatively smaller passage since the area requirements of the high-energy main stream will automatically be fulfilled first. Consider a condition where $M > 1.0$. If the main stream converged, an increase in pressure would be required which could not be traversed by the ejected flow. If the main stream flows straight through, or diverges in the mixing section, the area remaining for the ejected flow becomes very small so that choking of the ejected flow occurs for the contraction ratios and area distributions under consideration. (See fig. 4.) Thus the ejected flow rate is limited, and the tunnel cannot be expected to attain Mach numbers very much in excess of sonic. High values of tunnel pressure ratio are accompanied by a rearward expansion of a supersonic region into the diffuser. The main effect of this supersonic flow into the diffuser is that power requirements are increased; a secondary effect is that only small further increases in Mach number are possible since the ejector is operating near its maximum possible rate. If auxiliary pumping is allowed, the supersonic velocities near the diffuser entrance become less severe ($H_o/p_e = 1.545$, fig. 7(c)) and the Mach number increases as seen in figures 5(b) and 5(c).

Data for the sharp-slot cutoff (fig. 7(g)) did not extend through the mixing section, but from the data presented, the static pressure rise is very gradual for most of the range of tunnel pressure ratio and only slight differences exist between various values of m_b/m_o at a given H_o/p_e. At the highest value of H_o/p_e, a region of supersonic flow occurs near the upstream end of the diffuser and is followed by a rather sharp pressure gradient indicative of shock.

For the conditions using the open ejector, figures 7(h) and (i), the results are similar to those for the sharp-slot cutoff. The static pressure rise is very gradual. This rise suggests a rapidly thickening boundary layer, and at high H_o/p_e, a region of supersonic flow is found in the upstream region of the diffuser. This supersonic flow condition is somewhat aggravated with diffuser IV, figure 7(j), wherein there is a contraction of the diffuser very similar to that used previously in the mixing section. (See figs. 4 and 7(c).) Diffuser V, figure 7(k), however, showed only small regions of supersonic flow, most of which occurs in the mixing section, even at the highest tunnel pressure ratio. Any further increases in tunnel pressure ratio above the highest test value will be only slightly effective in increasing the Mach number, but will cause large reductions in diffuser static-pressure ratio.

Total pressure recovery of secondary flow at the ejector exit.- The total pressure of the secondary air at the ejector exit expressed in terms of free-stream pressure H_b/H_o is presented in figure 8 as a function of Mach number. These data were measured in the slots at the entrance to the mixing section for the shrouded configurations only; mixing with

the main stream precludes measurement of representative values for the secondary ejector flow in tests made with the open ejector. The data include all bleed-flow rates and flap angles except $\delta_F = 0^\circ$. Curves corresponding to recovery of from 0 to 40 percent of $(H_o - p_c)$ are also shown for comparison. Throughout most of the Mach number range, the measured values of secondary total pressure H_b indicate recovery of from 0.1 to 0.2 $(H_o - p_c)$. Higher recoveries up to 0.25 $(H_o - p_c)$ were obtained with the short shrouds and diffuser III at $M \approx 1.2$ and up to 0.45 $(H_o - p_c)$ with the short shrouds for $H_o/p_e \leqq 1.127$. The scatter noted in these data is a result of variations of the flap configurations and of the auxiliary bleed-flow rate. This scatter is small, and it is seen that the value of H_b/H_o is primarily a function of Mach number. Recent tests wherein a separate diffuser was used for the slot flow air (no ejector) have verified the pressure recoveries shown here and have further proved that this slot flow air can be successfully diffused to a very low velocity. Thus the sharp-slot-cutoff power requirements presented subsequently are not optimum, and further savings in power are possible when all slot flow air is used by a separate pumping system.

Total pressure distributions at the diffuser exit.- Total pressure distributions measured at the diffuser exit for all configurations except those with the long shrouds are presented in figure 9. Across the center of the stream, the exit total pressure ratio approached unity and decreased to a value approximating p_e/H_o at the walls. For diffusers I and II with short shrouds, constant area mixing, and divergent walls of the diffuser following the slotted walls of the tunnel, the exit pressure distributions in figures 9(a) and (b) indicate an asymmetry of flow which increases with tunnel pressure ratio. At H_o/p_e of approximately 1.9 the jet occupies about 1/2 of the diffuser cross section.

For diffuser III, with the same shroud and mixing-tube configuration as for diffusers I and II, losses at the duct center line were approximately the same as a normal shock loss at a Mach number corresponding to the minimum diffuser pressure p/H_o (fig. 7(f)). The distributions of total pressure were nearly symmetrical about the duct axis (figs. 9(c) and (d)), and no marked evidence of separation is present. Separation did occur, however, when this diffuser was tested in conjunction with the sharp-slot cutoff, figure 9(f); but, with an open ejector (boattailed slots), the separation was again eliminated, figures 9(g) to (i). At the highest values of H_o/p_e, for all distributions where flow symmetry is observed, there usually appears a dip in the profile near the diffuser center line, which is a phenomenon due to a normal shock and high losses on the duct center line with oblique shocks and low losses near the duct walls.

Power Requirements

The power required to operate this $4\frac{1}{2}$ - inch-square slotted tunnel has been calculated on the basis of adiabatic recompression of both the diffuser exit and auxiliary bleed flow to H_o. Expressed as the power parameter P/CT_o these results are presented as a function of Mach number in figures 10 and 12 and as a function of H_o/p_e in figure 11. The values of the power parameter shown in figure 10 are designated by a prime, $(P/CT_o)'$, to indicate conditions for which the main stream power was computed on the basis of the vertical survey at the diffuser exit only. These curves are not directly comparable with those of figures 11 and 12 since the latter are based on pressure surveys in both vertical and horizontal planes at the diffuser exit and thus include losses along the solid walls of the test section and the parallel walls of the diffuser. Within themselves, however, the curves of each group may be compared on a quantitative basis.

Effects of bleed-flow rate and tunnel pressure ratio.- At constant H_o/p_e, increasing Mach number is associated with increasing auxiliary bleed-flow rate as shown in figure 5. The overall power requirements of those configurations which utilize an ejector to return all or part of the slot flow to the main stream are presented for several configurations where the angle of the flaps was varied between 0° and 20°. The effect of changes in flap angle as shown in figures 10 and 12 varies with both ejector and diffuser geometry. With the short shroud and diffuser I, figures 10(a) to (c) and diffuser II, figures 10(d) to (f), increasing flap angle decreased the effect of tunnel pressure ratio. For values of H_o/p_e less than about 1.3, minimum power requirements for a constant δ_F were found to correspond to the conditions for zero auxiliary bleed flow. For values of $H_o/p_e > 1.3$, minimum power depended on flap angle. At $\delta_F = 0$, minimum power occurred at the minimum values of H_o/p_e at which the desired Mach number could be attained. At δ_F of 10° and 20°, minimum power for a given M was relatively independent of flow rate and tunnel pressure ratio.

In figure 11, the effects of tunnel pressure ratio and bleed flow on power are shown for $M = 1.41$. Here the auxiliary pumping power and main-stream power are shown, both separately and together, for the configuration with short shrouds and diffuser III. As the tunnel pressure ratio was increased, the bleed-flow rate was reduced to maintain constant M. As H_o/p_e increases, the main-stream power requirements also increase rather sharply, doubling in value between $H_o/p_e = 1.35$ and 1.9. The required auxiliary pumping power decreases rapidly (since the bleed-flow rate also decreases rapidly) with increasing H_o/p_e up to a value of approximately 1.60, which is near the condition for choked flow in the

[redacted]

diffuser. (See figs. 5 and 7(f).) Above this point, the bleed flow rate approaches a constant value of approximately 0.022; consequently, the auxiliary pumping power for fixed Mach numbers becomes constant. Increasing the tunnel pressure ratio above the condition for choking results in rapid increases in the power requirements.

The effect on power required of increasing the stream Mach number (through increasing the bleed flow rate) at constant tunnel pressure ratio can be seen in figure 12(a) for the configuration using short shrouds and diffuser III. For two values of H_o/p_e, 1.193 and 1.530, the auxiliary pumping power curves are shown separately, and appear to lie almost parallel to those of the overall tunnel power; therefore, increase in overall power with increased M is due primarily to the increased auxiliary pumping power requirements. This is in agreement with the near constancy in total pressure profile for constant H_o/p_e as seen in figure 9.

Effect of the sharp-slot cutoff.- Results of tests using the sharp-slot cutoff with diffuser III are shown in figure 12(b). It is seen that increasing H_o/p_e above about 1.18 results in rapid increases in the power requirements. From the static pressure distribution of figure 7(g) it is apparent that this increase in power is associated with the generation of supersonic velocities in the mixing section and diffuser at $H_o/p_e > 1.18$. Whereas the data of figure 12(b) were taken with auxiliary pumping only, the short shroud also provides a sharp-slot cutoff but slot flow air is pumped from the plenum by an ejector together with a vacuum pump.

The effects of ejector pumping are shown by a comparison of figure 12(b) with 12(a) where the flaps were deflected 10° and auxiliary pumping was used in conjunction with ejector pumping. At constant M the power requirements vary only slightly with H_o/p_e up to 1.64 as was seen in figure 11. At H_o/p_e greater than 1.64, the diffuser contains some regions of supersonic flow and further increases in tunnel pressure ratio cannot increase the pumping rate of the ejector; consequently, increases in H_o/p_e cause a shock to move downstream in the diffuser causing high losses and high power requirements.

Envelope curves of minimum power requirements are presented in figure 13. In figure 13(a), it can be seen that the improved bleed-flow pressure recovery obtainable with the ejector (shrouds) provides better power performance at low Mach numbers where only boundary-layer air must be handled through the slots and no shocks are present in the flow system. At $M > 1.0$, the configuration with 100 percent auxiliary bleed pumping (no ejector) becomes better due to improved diffuser total pressure recovery. Although these differences do not appear to be very great, it is interesting to note that an improvement in overall pressure recovery of only 2 percent will, for a tunnel operating at atmospheric total pressure and $T_o = 660°$ R, result in power savings of about 60 horsepower per square

foot of tunnel cross-sectional area; for a tunnel 8 feet in diameter, this represents a power saving of 3,000 horsepower.

Effect of open ejector exits.- The result of tests of $\delta_F = 0^\circ$, 10°, and 20° of the boattailed-slot exits are shown in figures 12(c), (d), and (e). At $\delta_F = 0^\circ$, the power requirements closely resemble those of figure 12(b), but are somewhat higher because of the lack of suitable fairing and high losses in the mixing section for the $\delta_F = 0^\circ$ condition. A comparison of figures 12(d) and 12(a) shows very little difference between the short shroud and boattailed-slot-exit configurations for $\delta_F = 10^\circ$, especially at $M < 1.35$.

Removal of the flat top sections from the floor bars from the downstream end of the bars forward a distance of one tunnel height produced the results shown in figures 12(f), (g), and (h). Envelope curves have been drawn for figures 12(c) to 12(h) and are shown in figures 13(b) and 13(c). Here, for δ_F of 10° and 20°, the power requirements are essentially equal for the two configurations. For $\delta_F = 0^\circ$, however, removal of the flats from the floor bars resulted in marked decreases in power for Mach numbers less than 1.1. It should be noted here that for a fixed δ_F of 10°, the least power requirement is associated with maximum bleed flow and the lowest possible H_o/p_e at the higher Mach numbers and is nearly insensitive to bleed-flow rates at the lower Mach numbers.

Diffuser effects.- Operation of configurations with short shrouds using the longer diffuser II did not appear to cause much change in power requirements over those of diffuser I (figs. 10(a) to 10(f)). For configurations using diffusers I and II, losses are based on surveys along only one axis of the exit and do not include losses associated with flow along the parallel walls of the diffuser and the unslotted walls of the tunnel. Although diffuser III with short shrouds, figure 12(a), appears to require more power than diffusers I or II with the same shrouds (figs. 10(b) and 10(e)), any direct comparison of the power requirements of these configurations is misleading because of the different total pressure survey arrangement. Diffuser III is considered superior in that the higher static pressure recoveries of figure 6 indicate better diffusion and the exit total pressure surveys indicate that the flow separation in diffusers I and II, figure 9, was eliminated in diffuser III.

In order to determine the effect of diffuser area ratio and divergence angle, the side walls of diffuser III were rotated inwardly about station zero toward the diffuser center line, reducing the area ratio from 1.97 to 1.52 for diffuser IV. Because of the curvature of the walls in the upstream end of the diffuser, this change of wall position resulted in a reduction in the minimum cross-sectional area of the diffuser as shown in figure 4. This diffuser, IV, was tested only with the configuration where the boattailed tops of the floor bars were removed and $\delta_F = 10^\circ$.

[redacted]

Results of tests with diffuser IV, shown in figure 12(i), follow the same trend as those with diffuser III, figure 12(g), and the envelope curves of minimum power for the two diffusers (fig. 13(d)) are in good agreement. Total-pressure profiles at the exit of these diffusers (see figs. 9(i) and (j)) show almost identical distributions up to the width of diffuser IV. The outboard edges of diffuser III contained only very low-velocity air which contributes little to the mass flow or total pressure recovery of the diffuser.

Diffuser V was formed to have the same contour as the upstream portion of III and the same area ratio as IV. The short length of diffuser V did not impair the maximum Mach number performance at the highest values of H_o/p_e but M was somewhat lower at intermediate values of H_o/p_e. (See figs. 5(h) and (k).) Static pressure ratios (see fig. 6(k)) were about the same as for diffuser IV which had a slightly lower peak than for III but with equal performance at high pressure ratios. The boundary layer for the short diffuser did not appear to separate and the center-stream distributions are flat with only small losses. (See fig. 9(l).) The power required for diffuser V, shown in figure 12(j), is the lowest of all the configurations tested; this is also shown in figure 13(d) where the minimum-power envelope curve for diffuser V is superimposed on those for diffusers III and IV. Above M of 1.35, the power required was less than that calculated for normal shock pressure loss in the main stream and loss of full dynamic pressure for the bleed air. Main-stream compression at better than normal shock efficiency is also indicated in figure 9(l) where H_e/H_o approached unity even at the highest Mach number.

Composite power curve envelopes.- A composite of the power envelope curves wherein the various flap angles have been consolidated wherever possible is presented in figure 14. Power requirements, based on total pressure recovery, show that the short, small-area-ratio diffuser is far superior to the other configurations and requires, on the average, only slightly more than one-half of the power of the next best configuration at the expense of a high exit velocity. Of the other configurations, the boattailed and the open boattails both with diffuser III appear best and the sharp-slot cutoff at M of 1.2 is equally good with the prospect of good efficiency at higher test Mach numbers if its test range could have been extended.

Although these performance curves, with the exception of the short, small-area-ratio diffuser, all appear to be nearly equal, the differences in power requirements can be appreciable as is shown in table II. This table was prepared on the basis of a tunnel operating at a stagnation temperature of 200° F with atmospheric total pressure. Here, at a Mach number of 1.2, the sharp-slot cutoff requires 394 hp/sq ft as compared with 415 hp/sq ft for the boattailed floor bar configuration. For an 8-foot test section, this would amount to a difference of approximately

[redacted]

1,000 hp. The short, small-area diffuser would operate at 217 hp/sq ft or 8,850 hp less than the sharp-slot cutoff at the expense of high diffuser exit velocities.

CONCLUSIONS

A $4\frac{1}{2}$-inch-square tunnel was tested to determine the effects of various slot exit shapes, mixing sections, and diffusers on power requirements. From these tests the following conclusions were formulated:

1. The use of shrouds or boattailed slots has little effect on performance.

2. Area contraction in the mixing section induced excessive supersonic velocities in the diffuser entrance and produced choking of the secondary flow from the ejector; auxiliary bleed-flow requirements were thereby increased.

3. A long diffuser with a curved entrance gave higher Mach numbers and diffuser static pressure rises than the shorter straight wall diffuser.

4. The curved-entrance diffuser with diverging walls downstream of the solid walls of the test section proved superior in Mach number and diffuser pressure rise performance to the diffuser with diverging walls downstream of the slotted walls of the test section.

5. The maximum test Mach number of the transonic tunnel without auxiliary bleed flow is dependent upon the geometry of the air passages downstream of the slotted portions of the test section and is limited by choking. The maximum test Mach number is increased as the bleed flow is increased by using auxiliary pumping.

6. The most efficient method of obtaining the maximum Mach number within the slotted test section is through a combination of auxiliary pumping and ejector pumping.

Langley Aeronautical Laboratory,
National Advisory Committee for Aeronautics,
Langley Field, Va., March 5, 1956.

[redacted]

REFERENCES

1. Whitcomb, Richard T., Carmel, Melvin M., and Morgan, Francis G., Jr.: An Investigation of the Stream-Tube Power Losses and an Improvement of the Diffuser-Entrance Nose in the Langley 8-Foot Transonic Tunnel. NACA RM L52E20, 1952.

2. Dennard, John S.: A Preliminary Investigation of the Power Requirements of Slotted Test Sections. NACA RM L53F10, 1953.

3. Dennard, John S., and Little, Barney H., Jr.: Effects of Auxiliary and Ejector Pumping on the Mach Number Attainable in a $4\frac{1}{2}$- by $4\frac{1}{2}$- Inch Slotted Tunnel at Low Pressure Ratios. NACA RM L53K19, 1954.

4. Little, B. H., Jr., and Cubbage, James M., Jr.: Effects of Combining Auxiliary Bleed With Ejector Pumping on the Power Requirements and Test-Section Flow of an 8-Inch by 8-Inch Slotted Tunnel. NACA RM L55E25, 1955.

[redacted]

TABLE I

ORDINATES FOR CURVED WALL DIFFUSERS

Diffuser I (15.56-inch long straight walls)			Diffuser II (24-inch long, curved upper and lower walls)			Diffuser III (24-inch long, curved side walls)			Diffuser IV (24-inch long, curved side walls)			Diffuser V (12.25-inch long, curved side walls)		
X	Y	Z	X	Y	Z	X	Y	Z	X	Y	Z	X	Y	Z
0	2.75	2.250	0	2.750	2.250	0	2.750	2.250	0	2.750	2.250	0	2.750	2.250
Varies linearly	Varies linearly	Constant	1.0	2.752	Constant	1.0	Constant	2.252	1.0	Constant	2.217	1.0	Constant	2.252
			2.0	2.760		2.0		2.258	2.0		2.189	2.0		2.258
			3.0	2.770		3.0		2.268	3.0		2.164	3.0		2.268
			4.0	2.793		4.0		2.287	4.0		2.149	4.0		2.287
			5.0	2.840		5.0		2.324	5.0		2.151	5.0		2.324
			6.0	2.950		6.0		2.372	6.0		2.164	6.0		2.372
			7.0	2.975		7.0		2.434	7.0		2.192	7.0		2.434
			8.0	3.053		8.0		2.499	8.0		2.222	8.0		2.499
			9.0	3.128		9.0		2.569	9.0		2.258	9.0		2.569
			10.0	3.231		10.0		2.642	10.0		2.306	10.0		2.642
15.56	4.50		24.0	4.437		24.0		3.630	24.0		2.800	12.25		2.802
Area ratio, 2:1 Equiv. conical angle, 5.76° Wall divergence angle, 12.833°			Area ratio, 1.97:1 Equiv. conical angle, 3.59° Wall divergence angle, 9.85°			Area ratio, 1.97:1 Equiv. conical angle, 3.59° Wall divergence angle, 8.067°			Area ratio, 1.52:1 Equiv. conical angle, 1.55° Wall divergence angle, 4.033°			Area ratio, 1.52:1 Equiv. conical angle, 3.06° Wall divergence angle, 8.133°		

TABLE II

POWER REQUIREMENTS FOR A SLOTTED TUNNEL OPERATING

WITH ATMOSPHERIC TOTAL PRESSURE

[T_o = 660° R]

M	Power requirement in horsepower per square foot of throat area				
	Diffuser III with -				Diffuser V with opened slots in downstream end of test section
	Sharp-slot cutoff	Short shrouds	Boattailed floor bars	Opened slots in downstream end of test section	
0.7	165	127	110	124	58
.8	195	169	142	140	77
.9	230	215	190	164	95
1.0	277	277	238	220	128
1.1	325	344	307	307	167
1.2	394	443	415	425	217
1.3	---	580	558	558	286
1.4	---	768	740	716	386
1.5	---	1,026	947	910	520

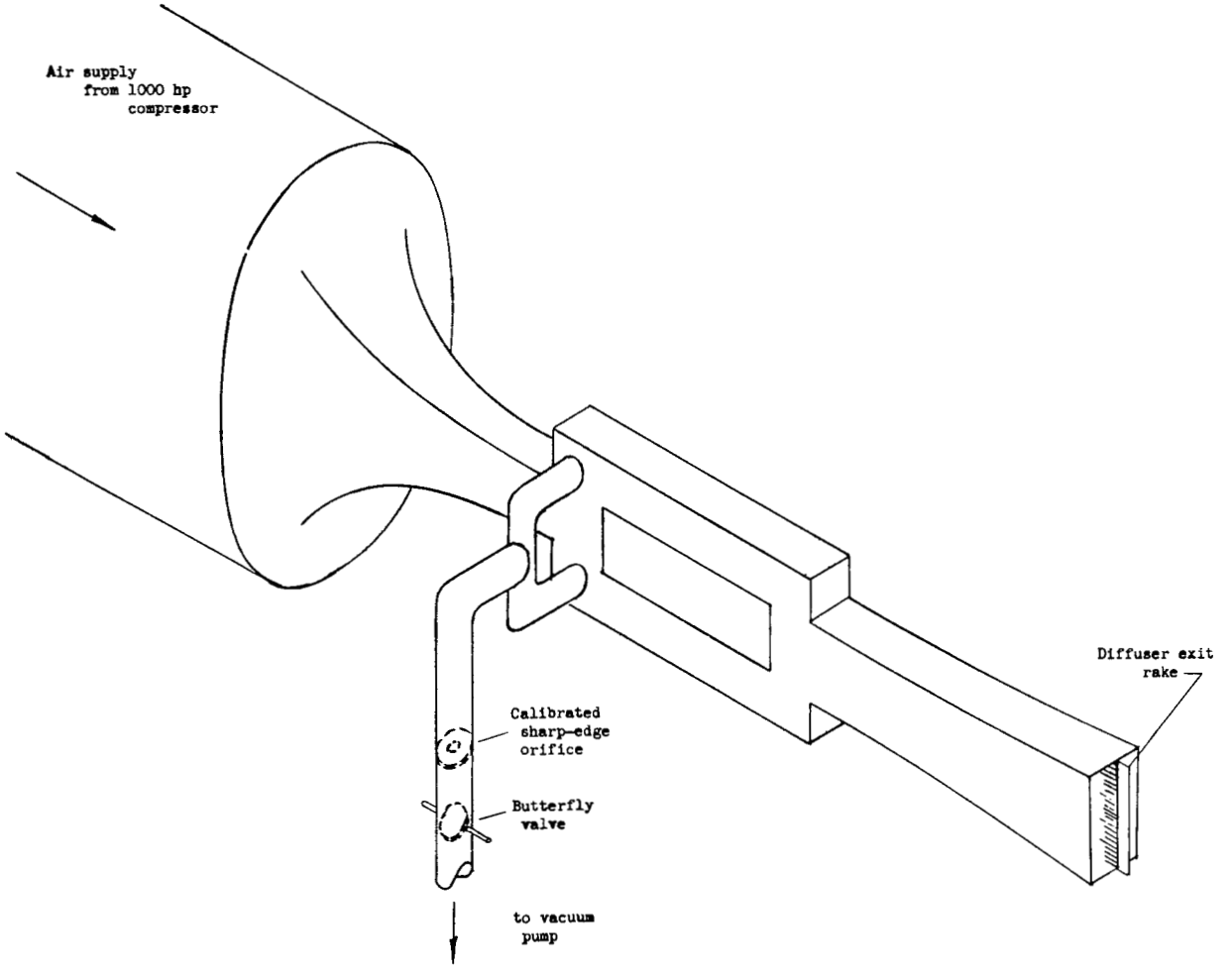

Figure 1.- General arrangement of flow system showing air supply, vacuum pump connections, and diffuser exit rake.

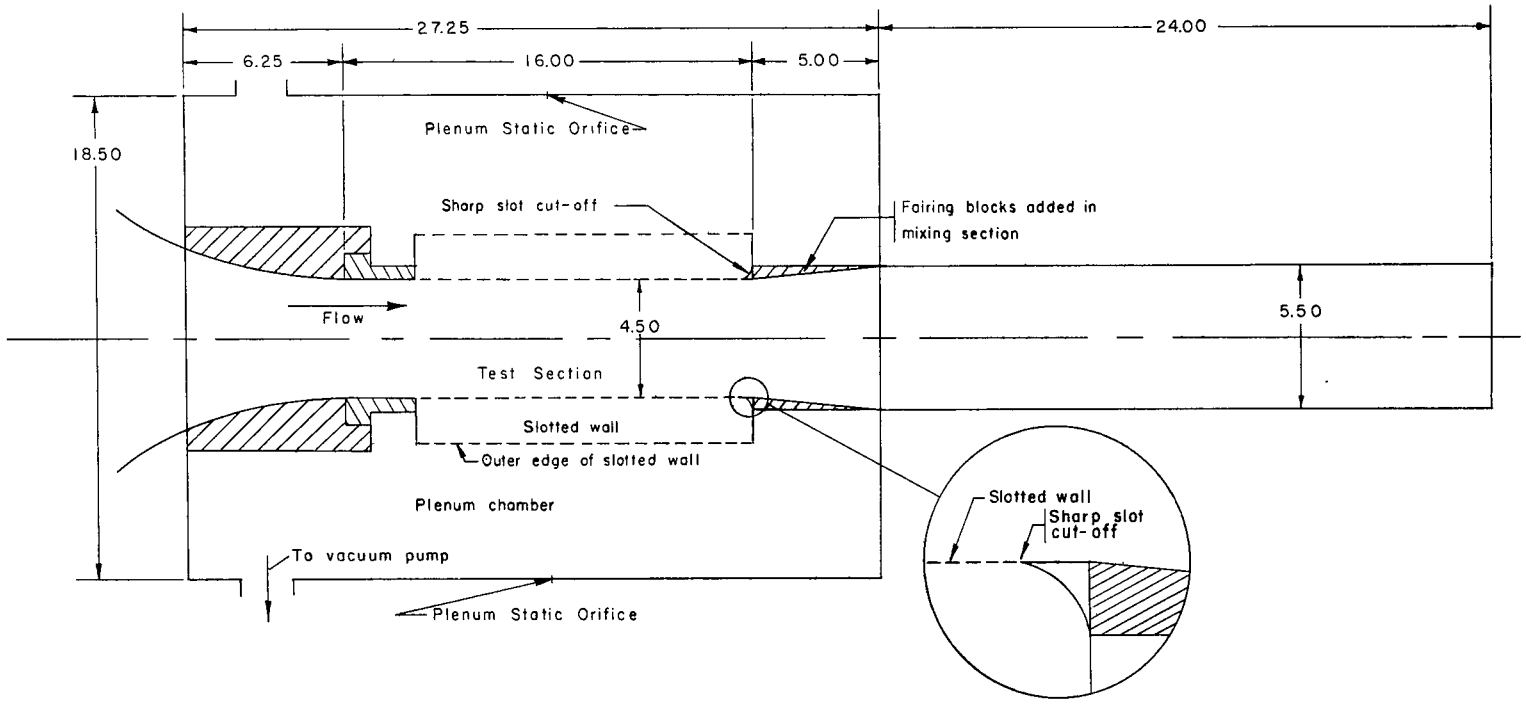

Figure 2.- Line drawing of the general arrangement and principal dimensions of the test setup showing the sharp-slot cutoff with diffuser III and fairing blocks in the mixing section.

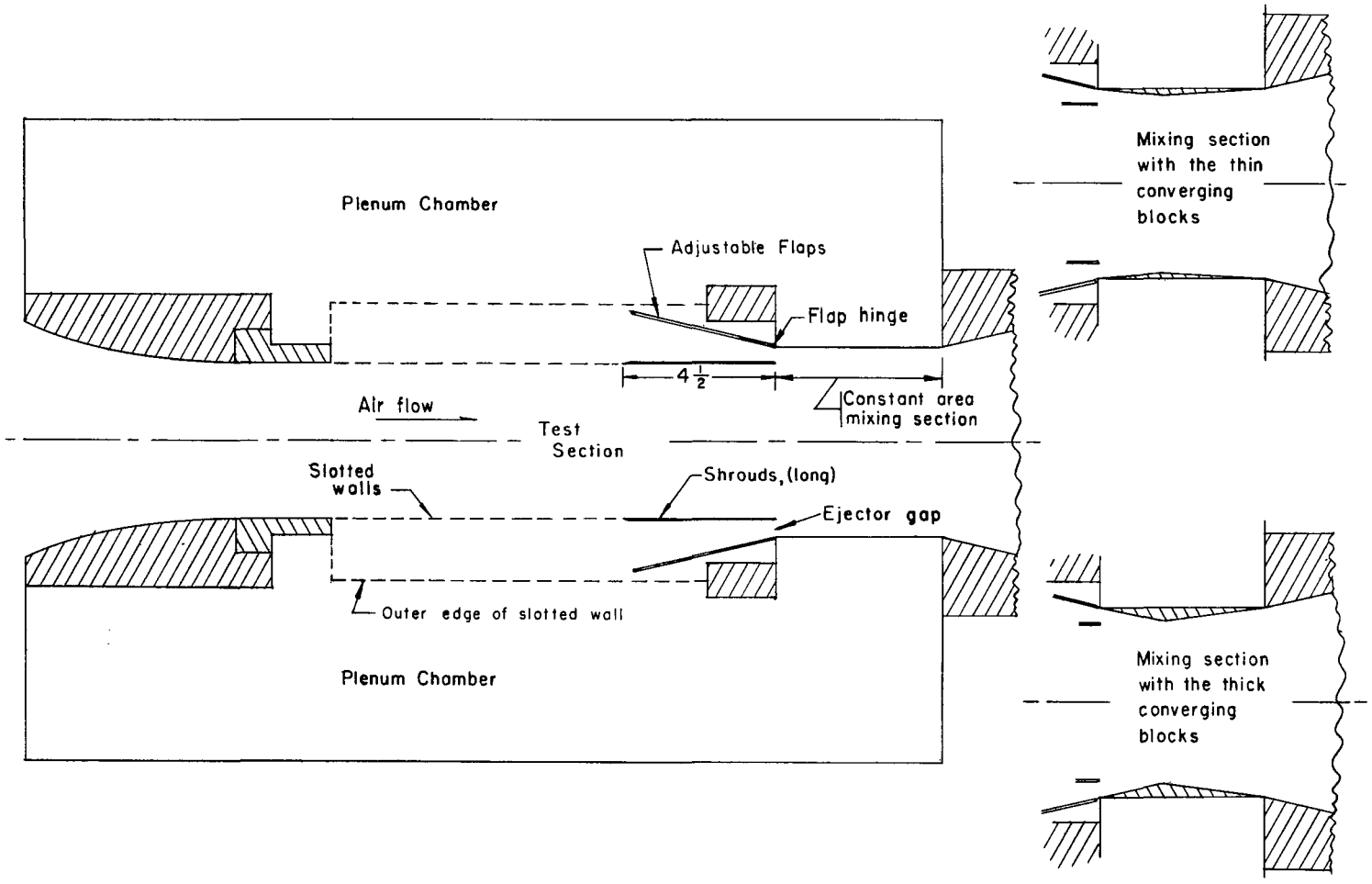

(a) Long shrouds with constant area (and with converging) mixing sections.

Figure 3.- Line drawings of the various test configurations.

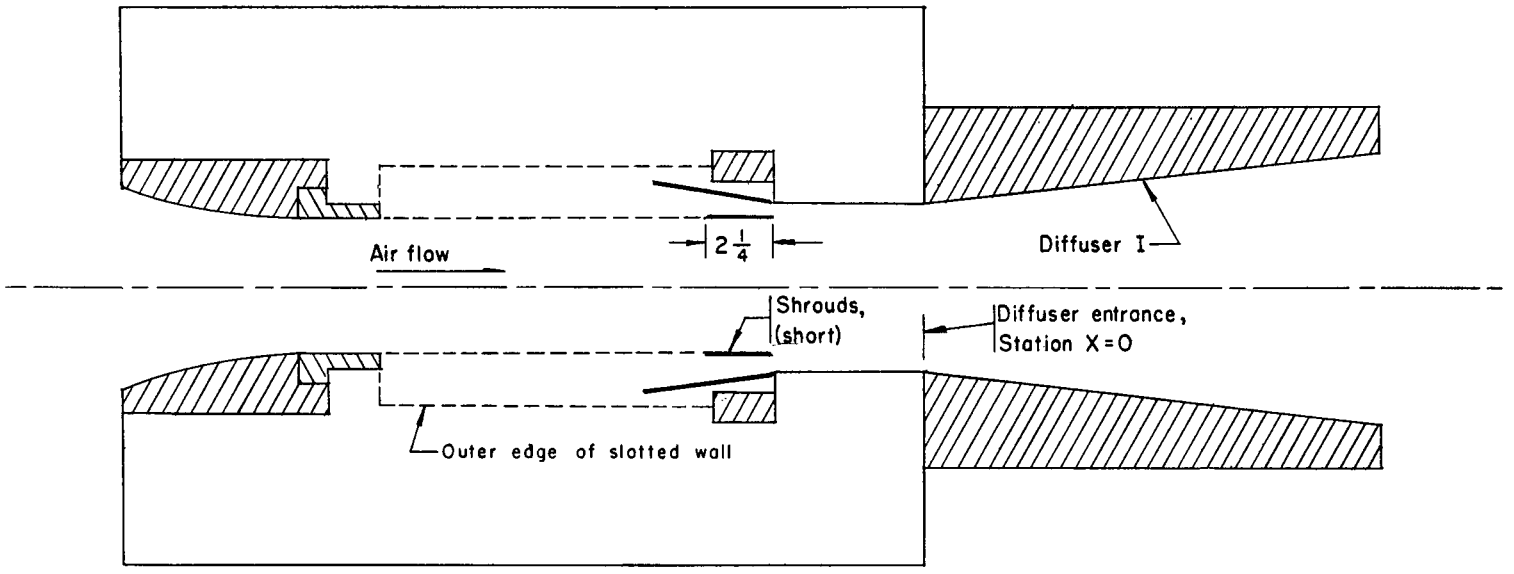

(b) Short shrouds with diffuser I installed.

Figure 3.- Continued.

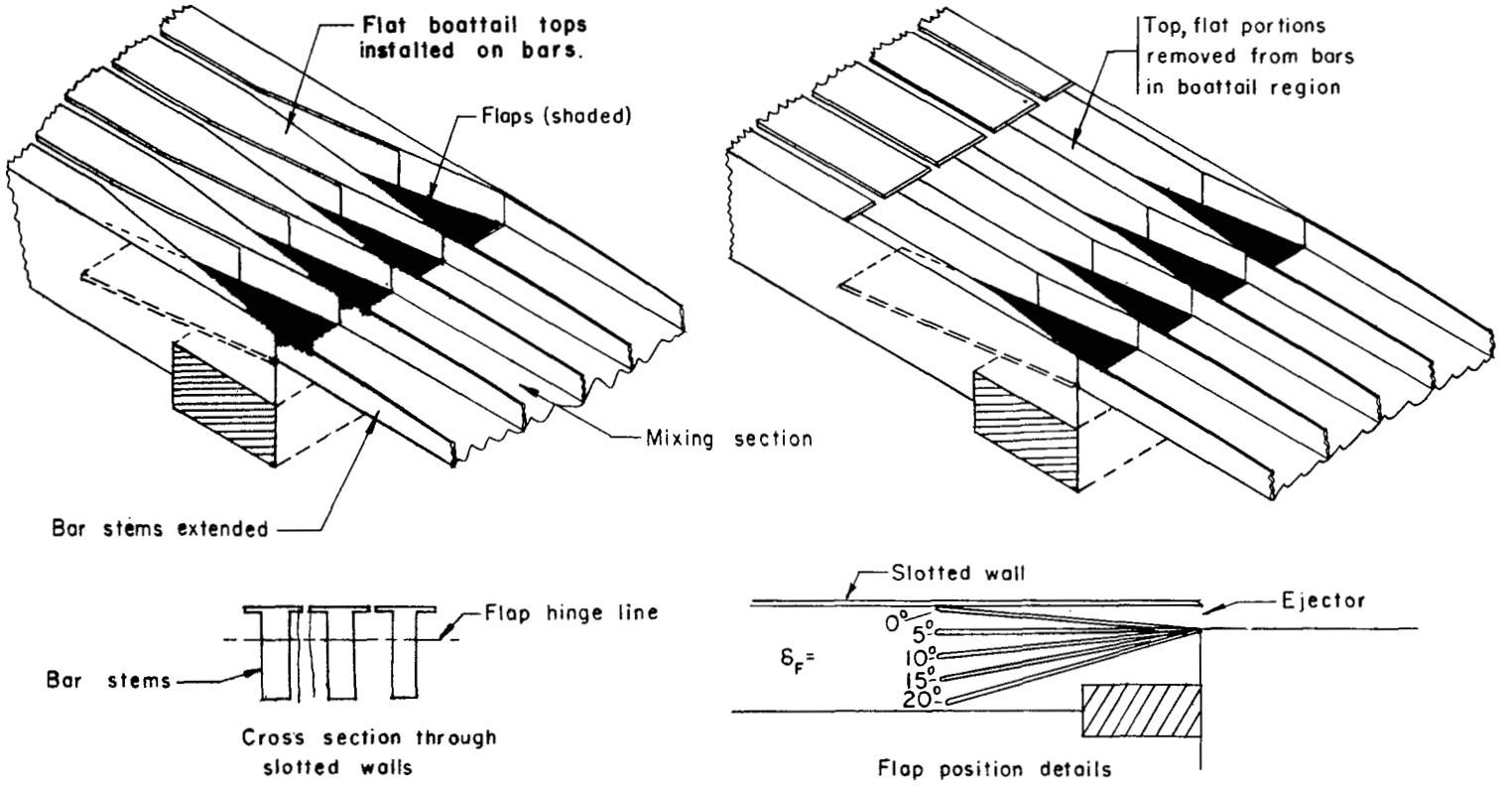

(c) Details of boattail bars and of the slotted wall and flap arrangements.

Figure 3.- Concluded.

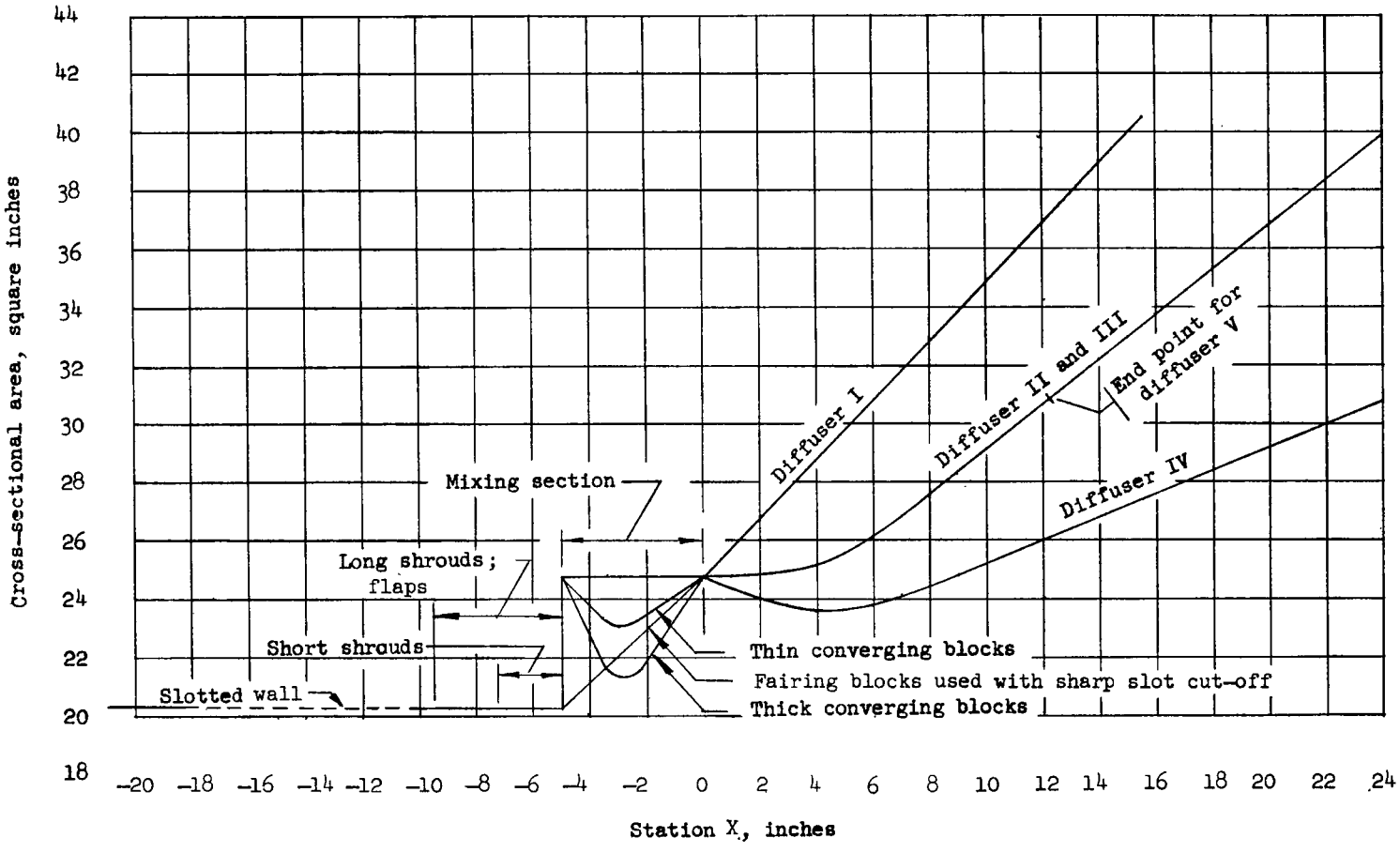

Figure 4.- Variation of tunnel cross-sectional area with length for the several test conditions.

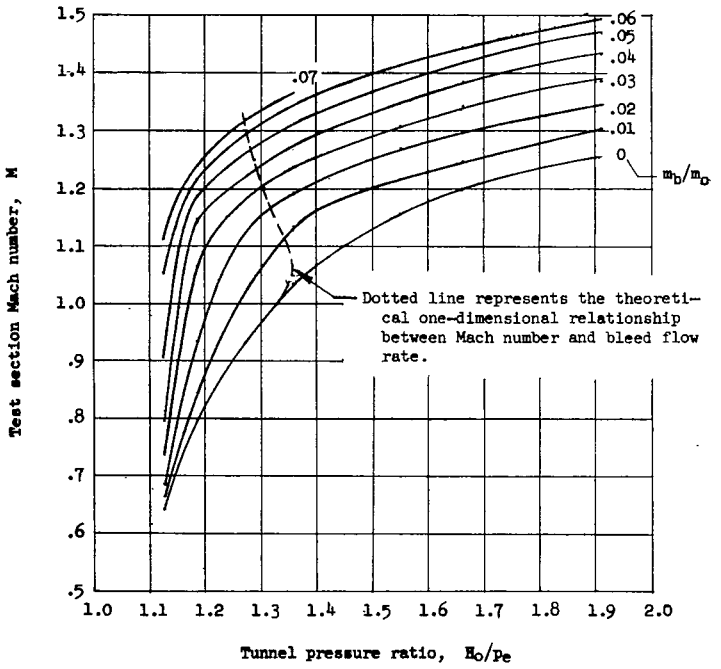

(a) Long shrouds and diffuser I. $\delta_F = 10^\circ$; constant area mixing.

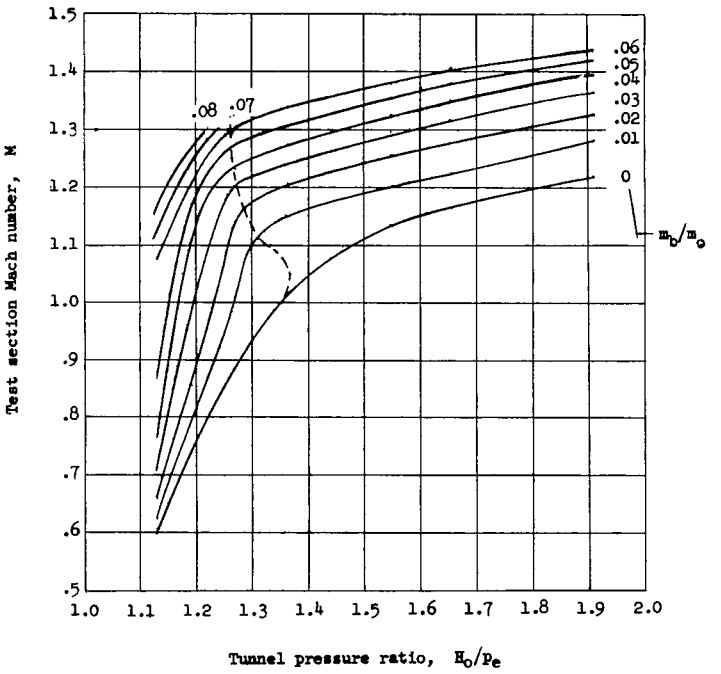

(b) Long shrouds and diffuser I with thin converging blocks in mixing section. $\delta_F = 10^\circ$.

Figure 5.- Variation of Mach number with tunnel pressure ratio for several bleed-flow rates.

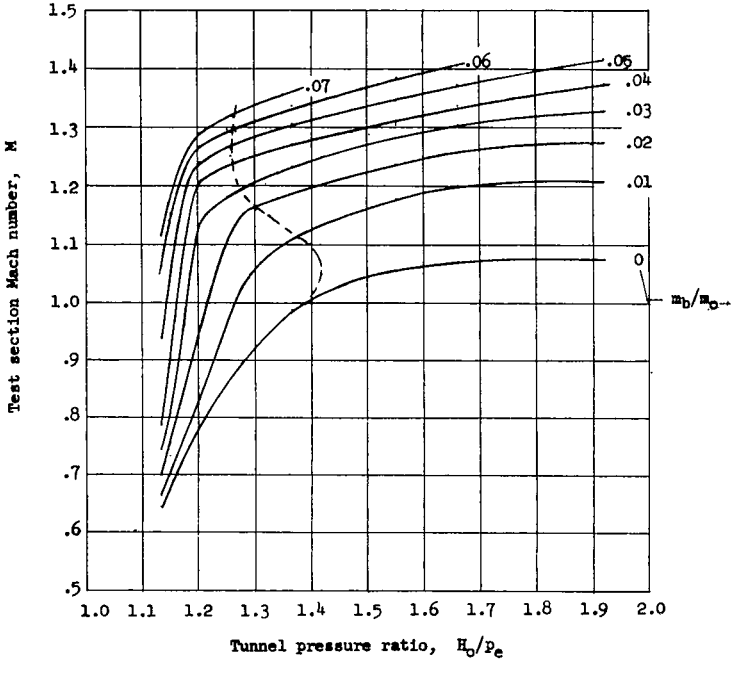

(c) Long shrouds and diffuser I with thick converging blocks in mixing section. $\delta_F = 10^o$.

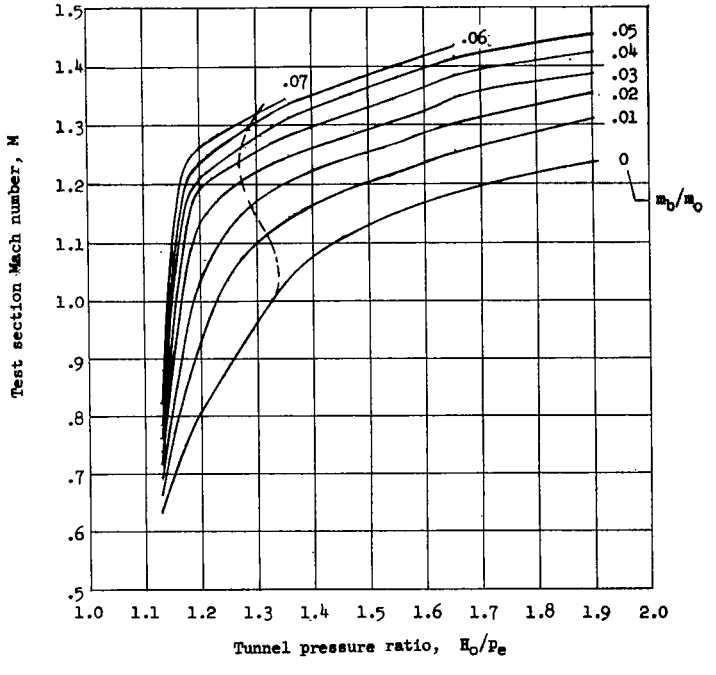

(d) Short shrouds and diffuser I. $\delta_F = 10^o$; constant area mixing.

Figure 5.- Continued.

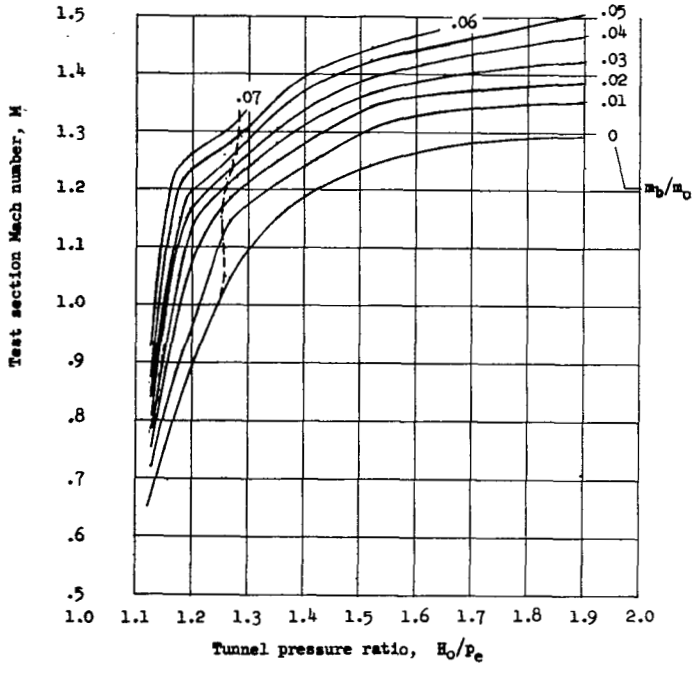

(e) Short shrouds and diffuser II. $\delta_F = 10^\circ$; constant area mixing.

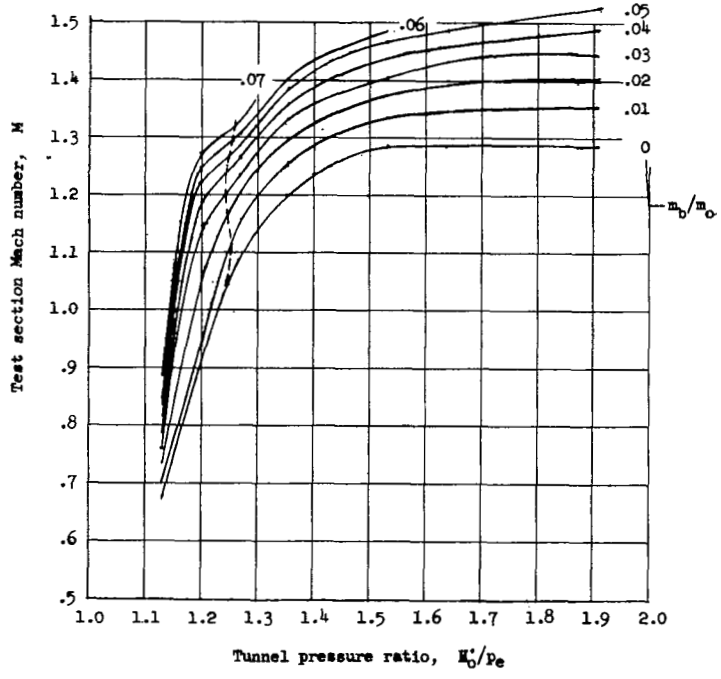

(f) Short shrouds and diffuser III. $\delta_F = 10^\circ$; constant area mixing.

Figure 5.- Continued.

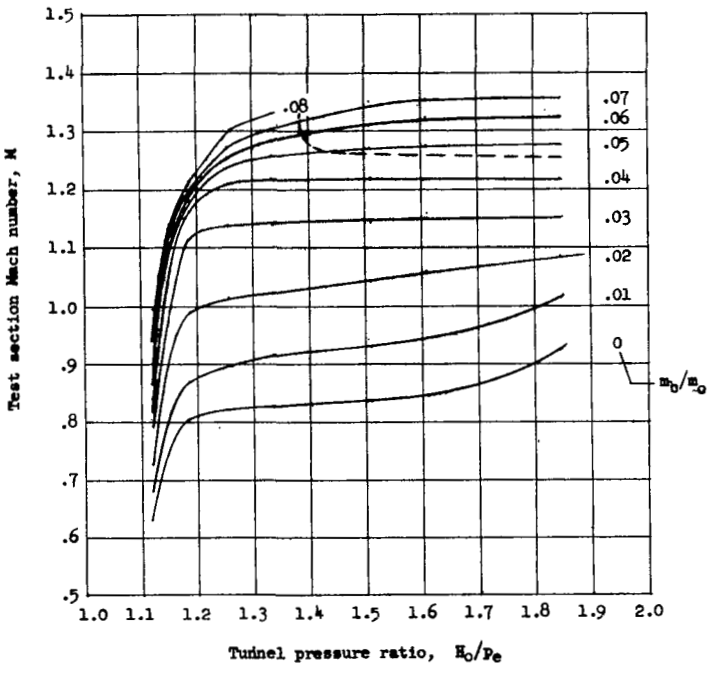

(g) Sharp-slot cutoff without flaps. Diffuser III faired through mixing section to surface of slotted floor, all slot flow air removed by auxiliary pumping.

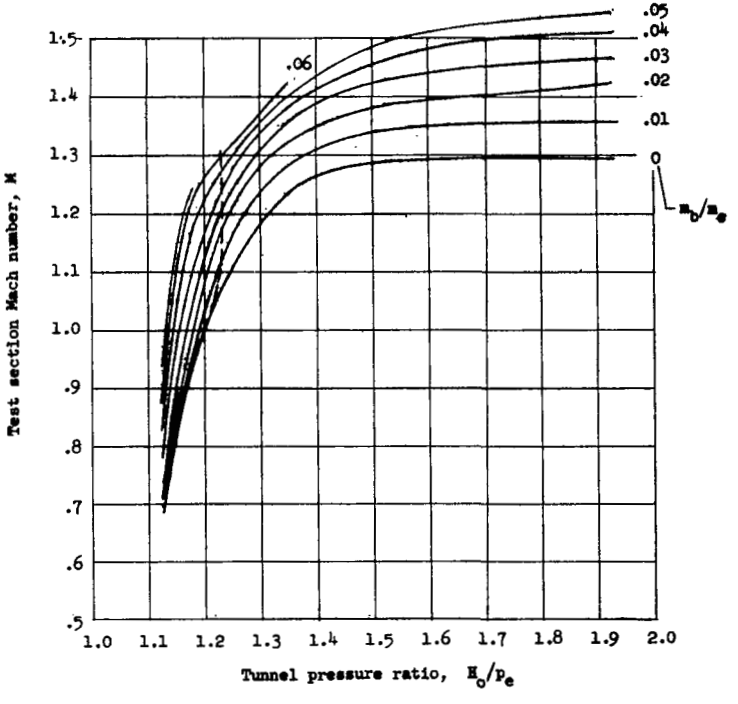

(h) Boattailed slots with diffuser III. $\delta_F = 10^\circ$; constant area mixing.

Figure 5.- Continued.

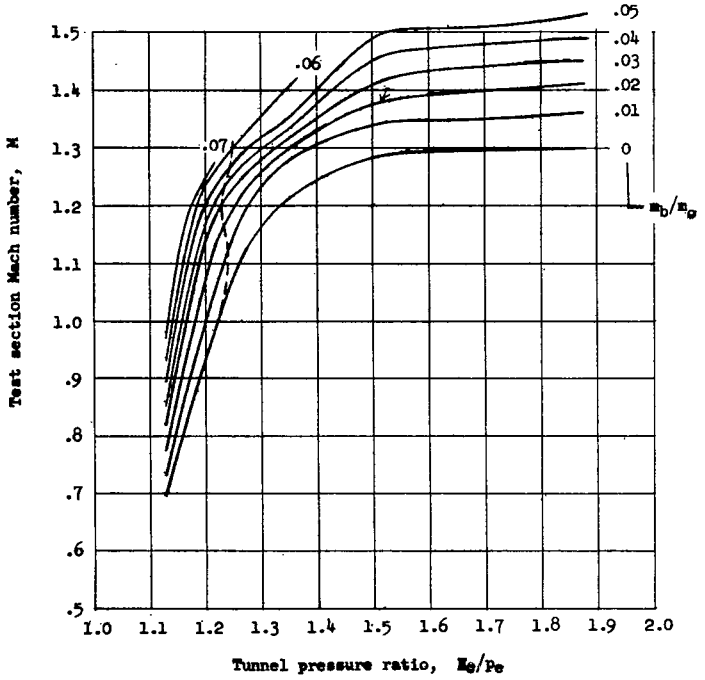

(i) Flats removed from boattail region. Diffuser III; $\delta_F = 10^o$; constant area mixing.

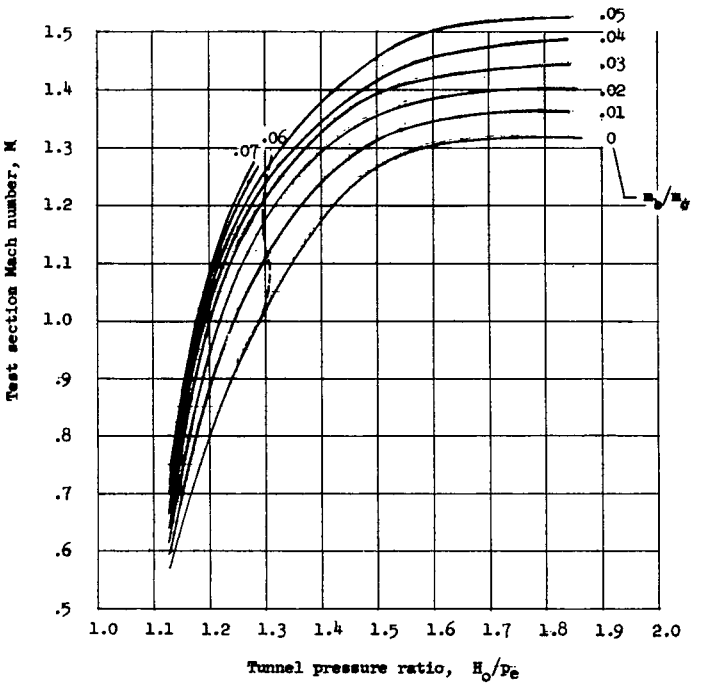

(j) Flats removed from boattail region. Diffuser IV; $\delta_F = 10^o$; constant area mixing.

Figure 5.- Continued.

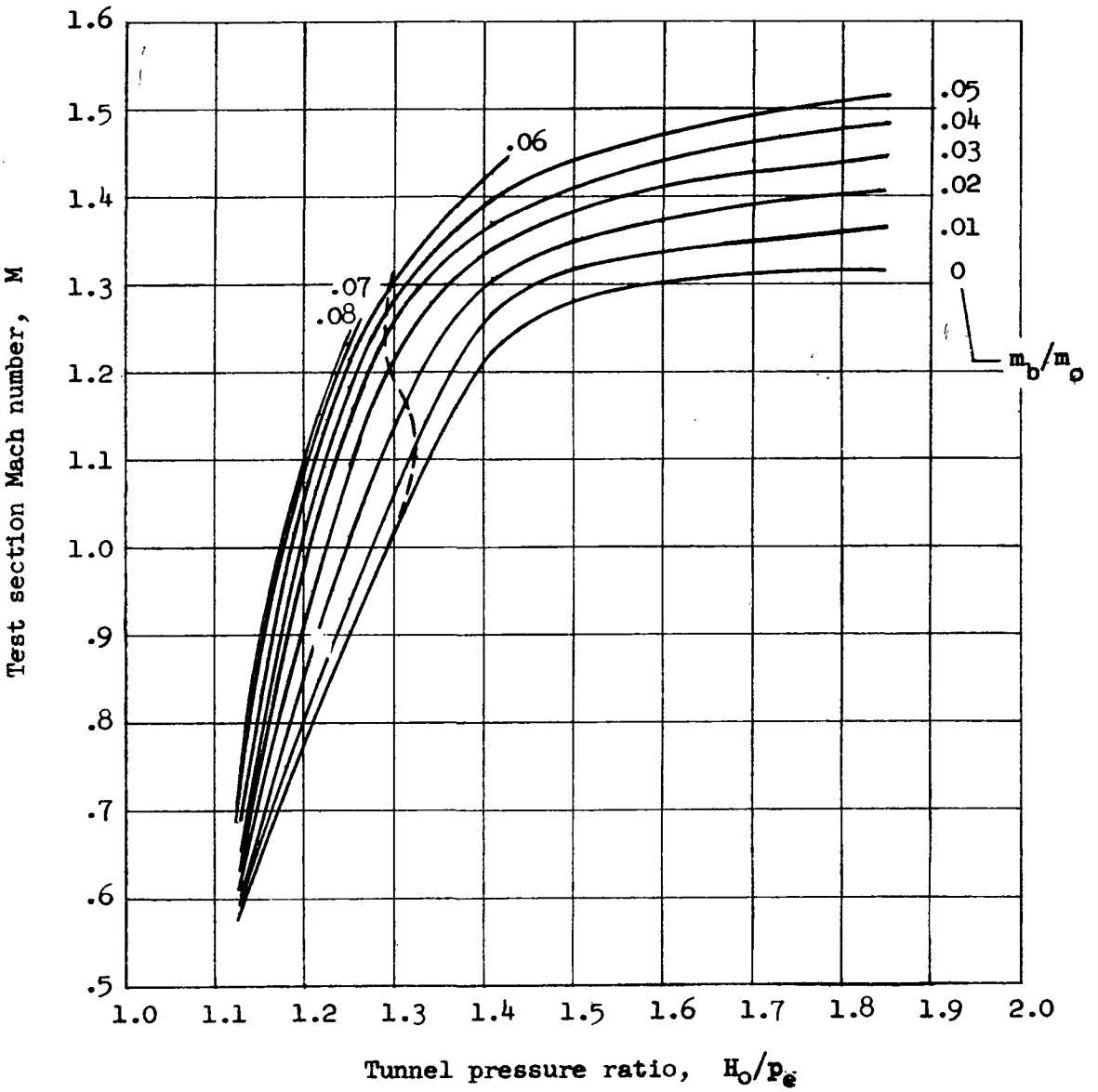

(k) Flats removed from boattail region. Diffuser V; $\delta_F = 10^\circ$; constant area mixing.

Figure 5.- Concluded.

[redacted]

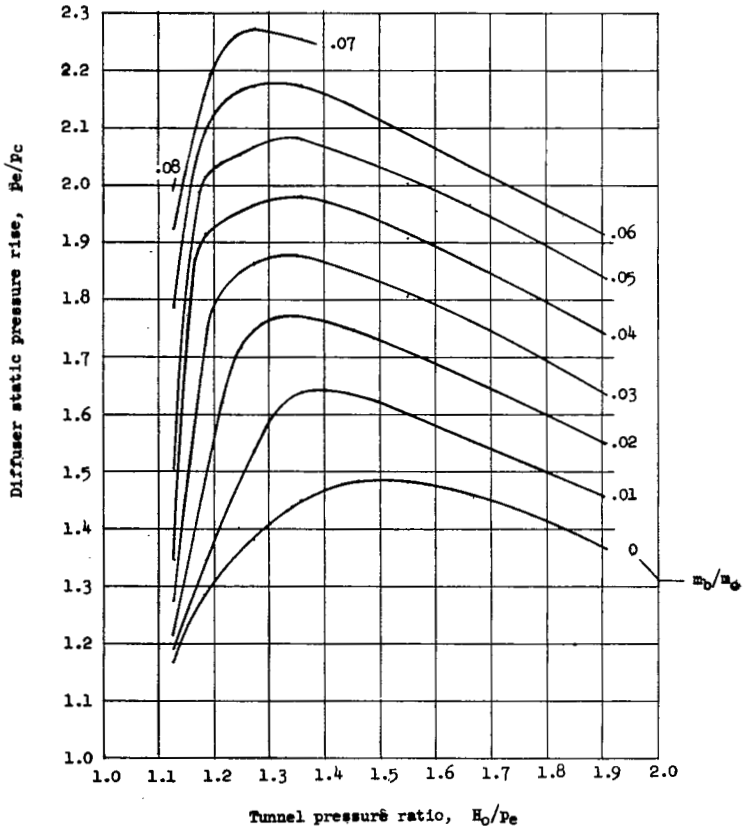

(a) Long shrouds and diffuser I. $\delta_F = 10^\circ$; constant area mixing.

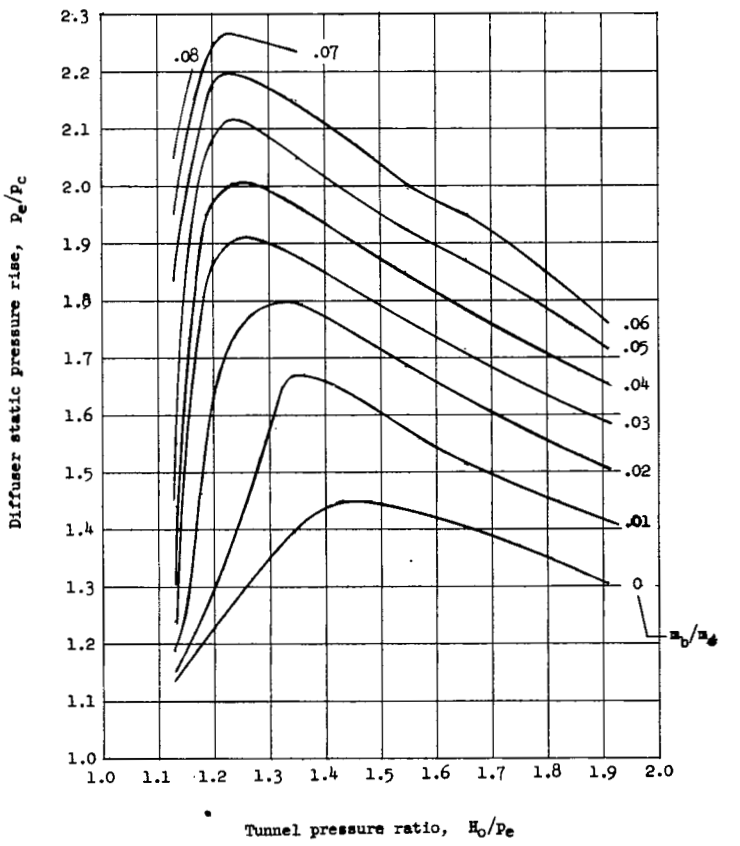

(b) Long shrouds and diffuser I with thin converging blocks in mixing section. $\delta_F = 10^\circ$.

Figure 6.- Variation of diffuser exit to test section static pressure ratio with tunnel pressure ratio for several values of auxiliary bleed-flow rate.

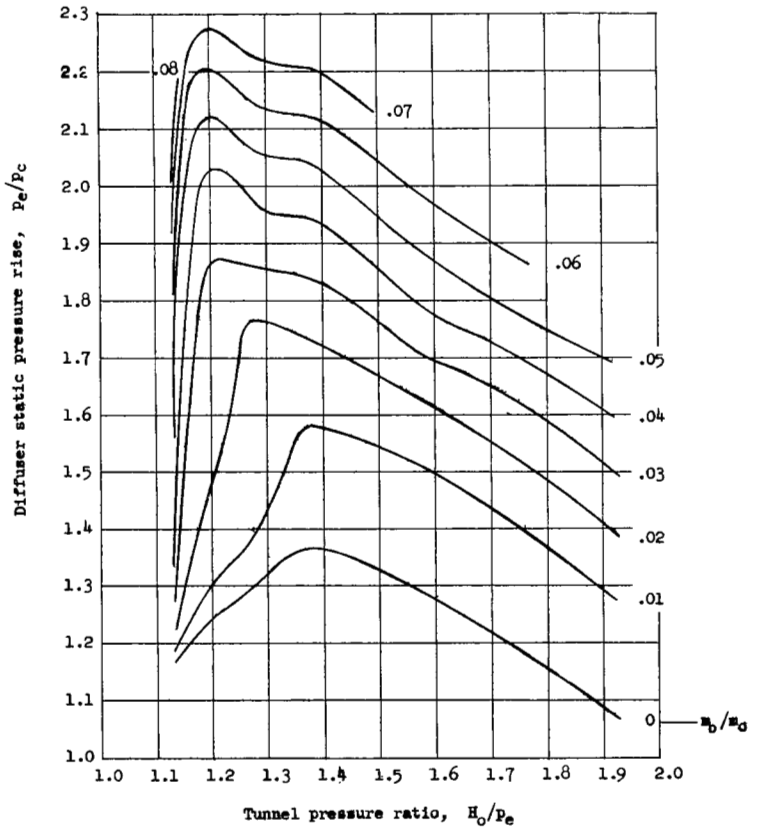

(c) Long shrouds and diffuser I with thick converging blocks in mixing section. $\delta_F = 10^o$.

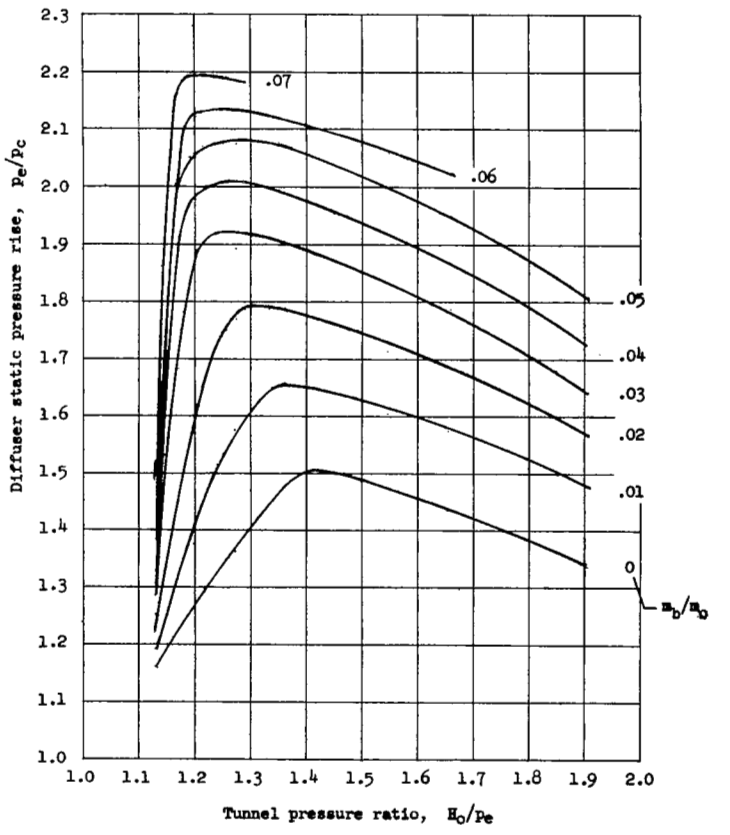

(d) Short shrouds and diffuser I. $\delta_F = 10^o$; constant area mixing.

Figure 6.- Continued.

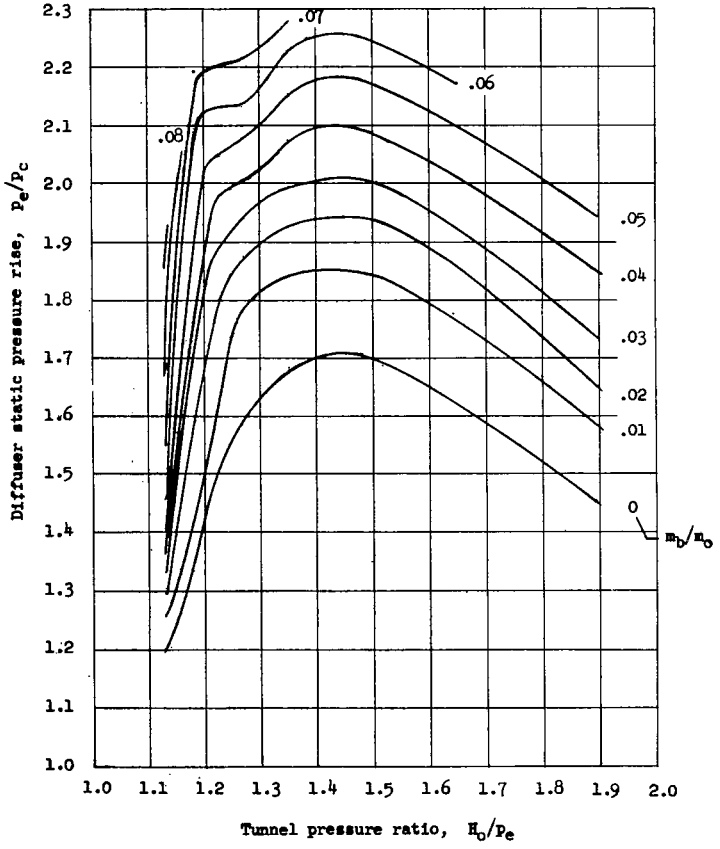

(e) Short shrouds and diffuser II. $\delta_F = 10^\circ$; constant area mixing.

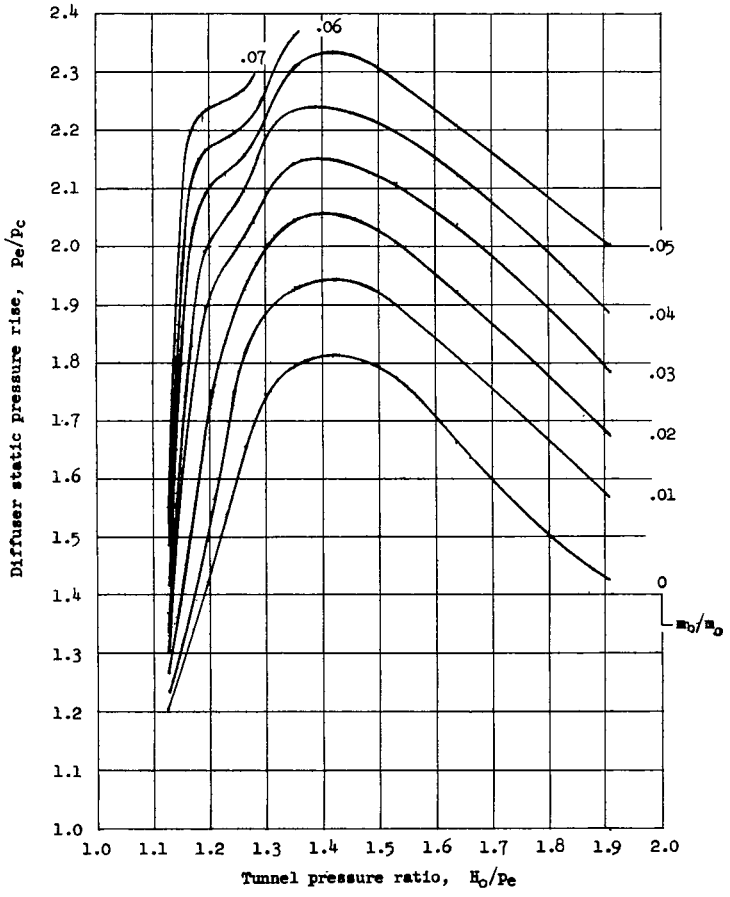

(f) Short shrouds and diffuser III. $\delta_F = 10^\circ$; constant area mixing.

Figure 6.- Continued.

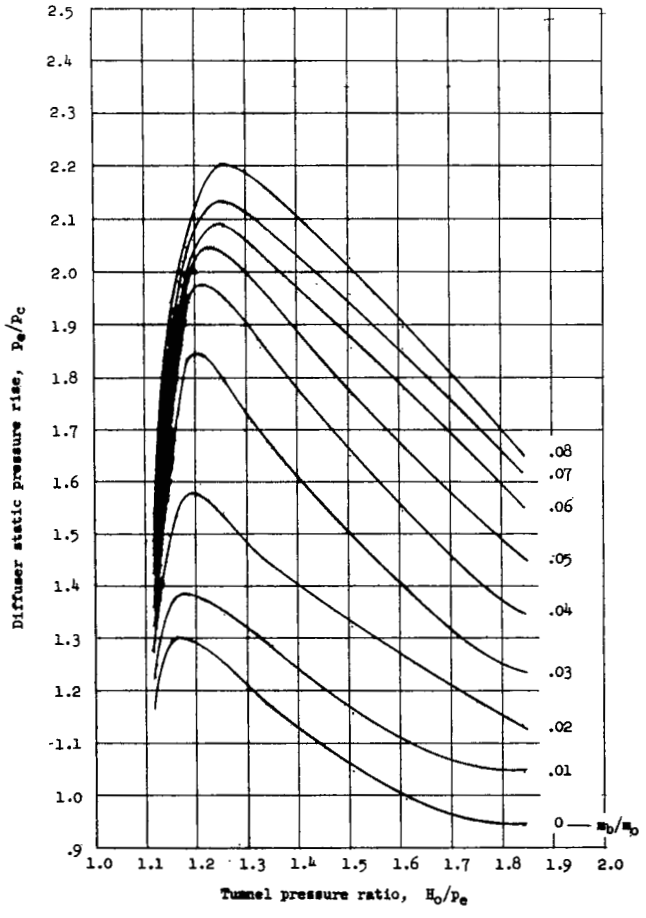

(g) Sharp-slot cutoff without flaps. Diffuser III faired through mixing section to surface of slotted floor; all slot flow air removed by auxiliary pumping.

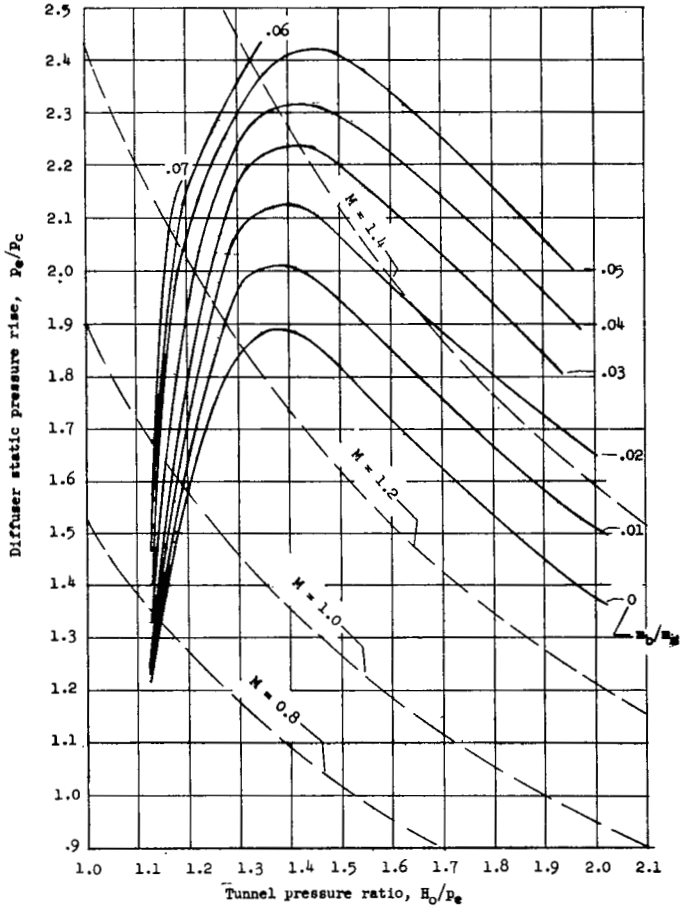

(h) Boattailed slots with diffuser III. $\delta_F = 10^\circ$; constant area mixing.

Figure 6.- Continued.

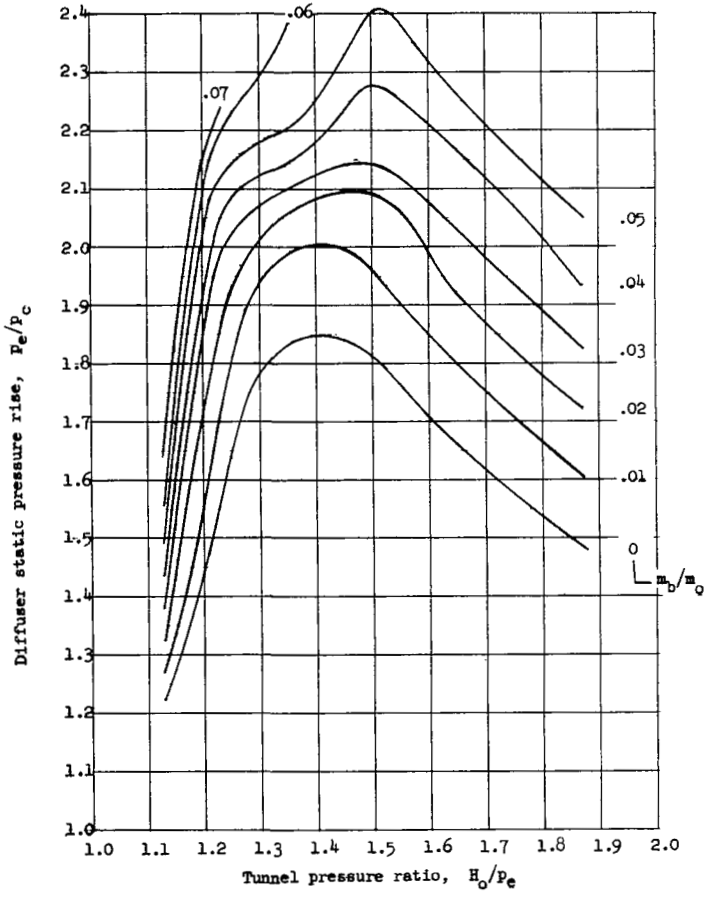

(i) Flats removed from boattail region. Diffuser III; $\delta_F = 10^o$; constant area mixing.

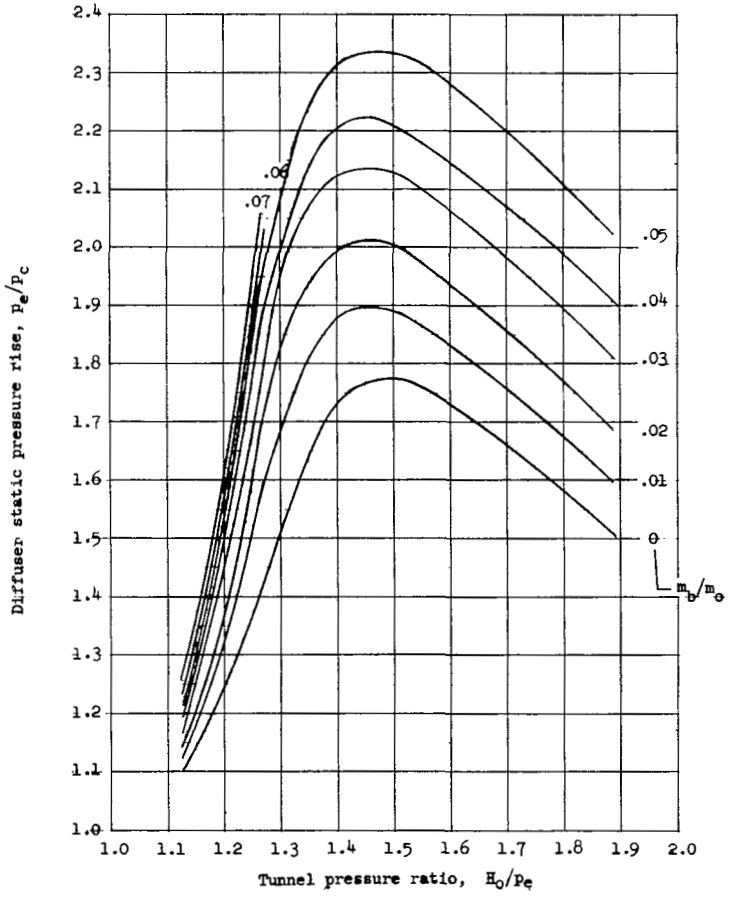

(j) Flats removed from boattail region. Diffuser IV; $\delta_F = 10^o$; constant area mixing.

Figure 6.- Continued.

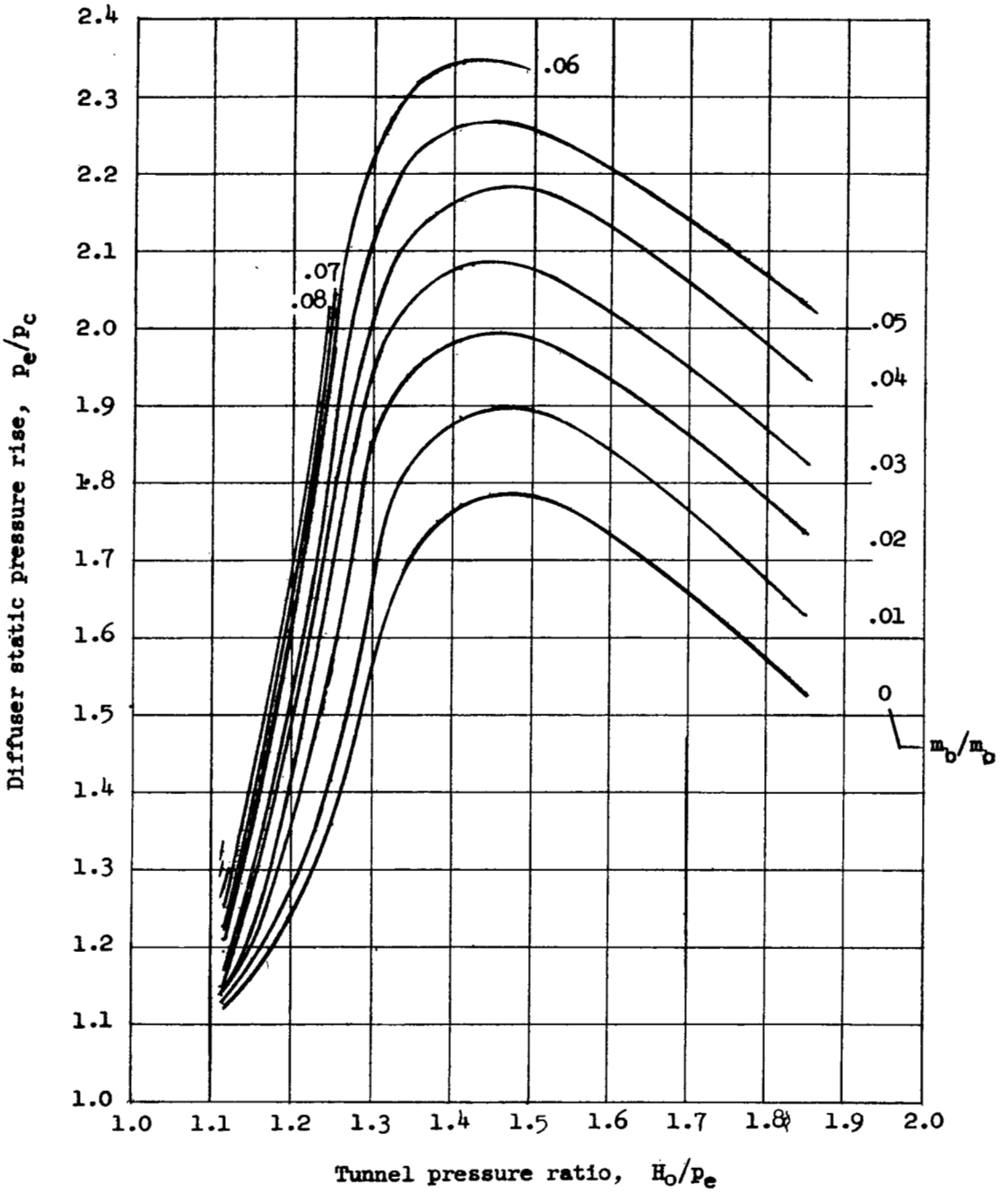

(k) Flats removed from boattail region. Diffuser V; $\delta_F = 10^\circ$; constant area mixing.

Figure 6.- Concluded.

[redacted]

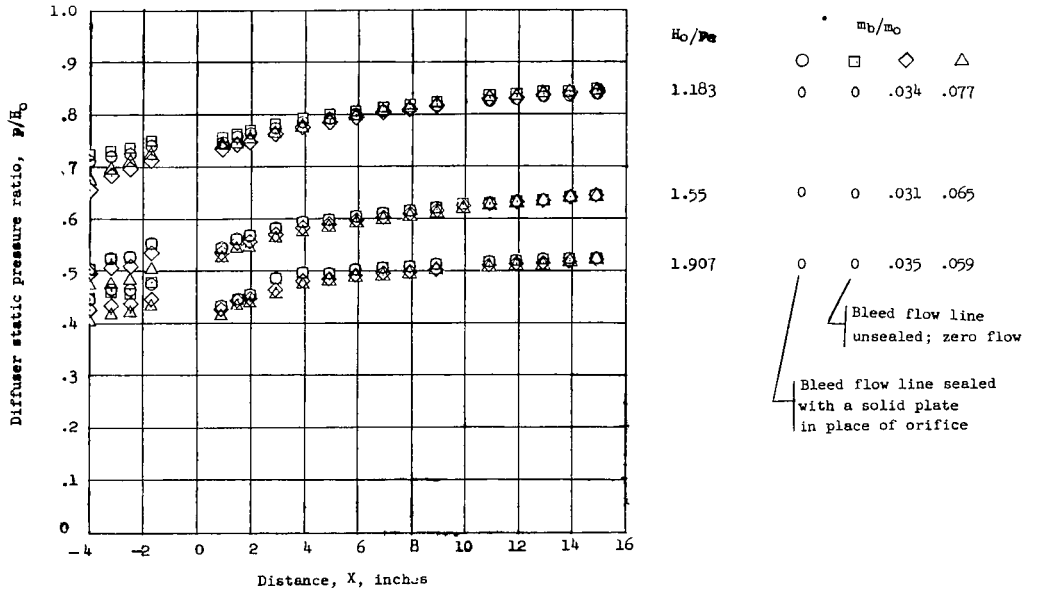

(a) Long shrouds. Diffuser I; $\delta_F = 10^\circ$; constant area mixing.

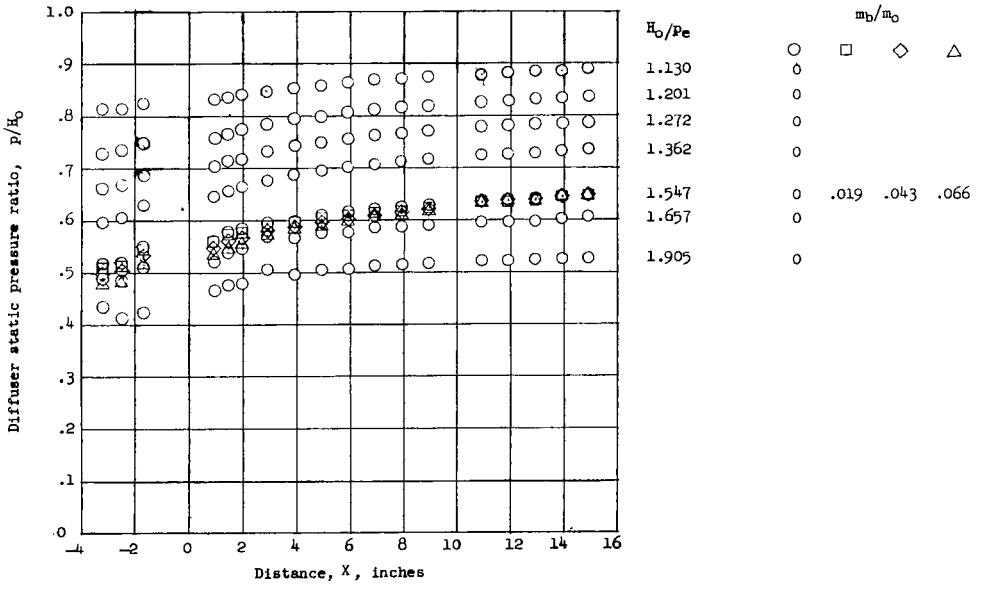

(b) Long shrouds. Diffuser I with thin converging blocks in mixing section; $\delta_F = 10^\circ$.

Figure 7.- Longitudinal variation of static pressure in the diffuser for several values of tunnel pressure ratio and bleed-flow rates.

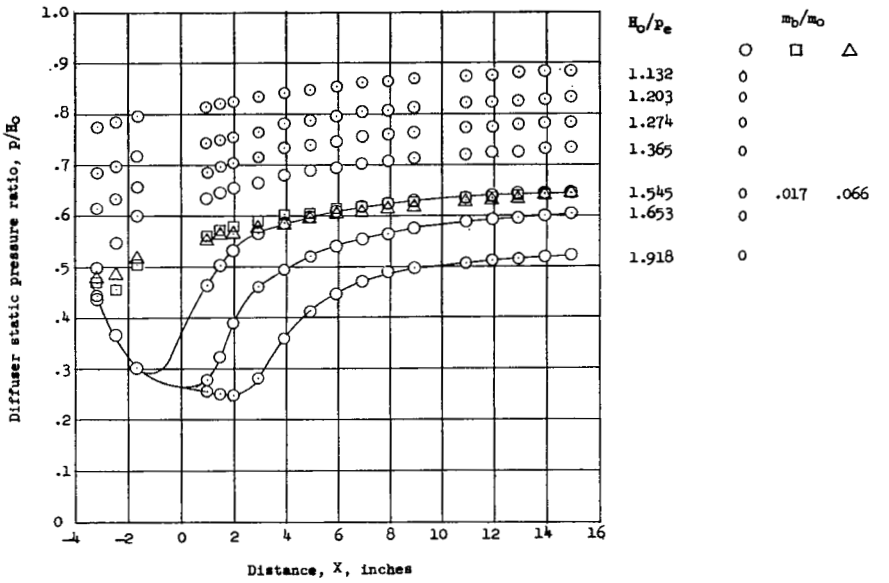

(c) Long shrouds. Diffuser I with thick converging blocks in mixing section; $\delta_F = 10^\circ$.

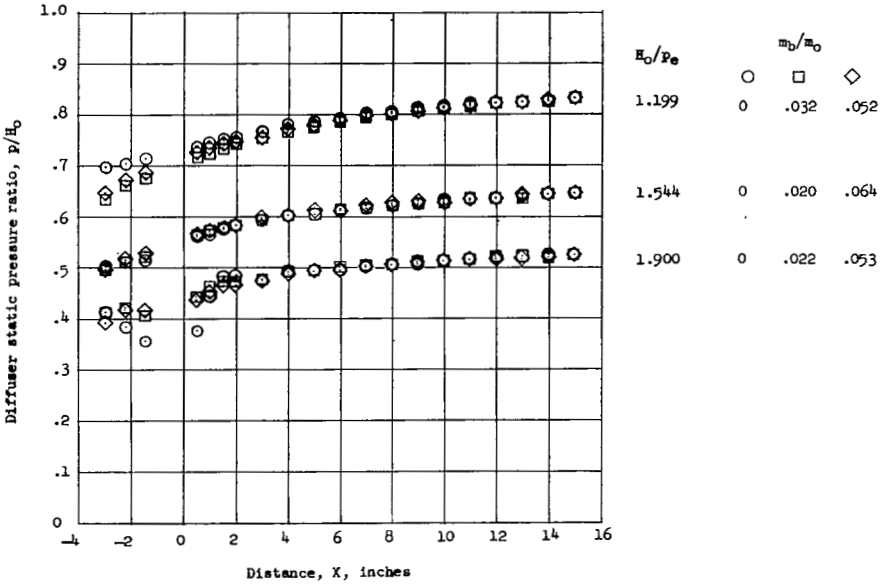

(d) Short shrouds. Diffuser I; $\delta_F = 10^\circ$; constant area mixing.

Figure 7.- Continued.

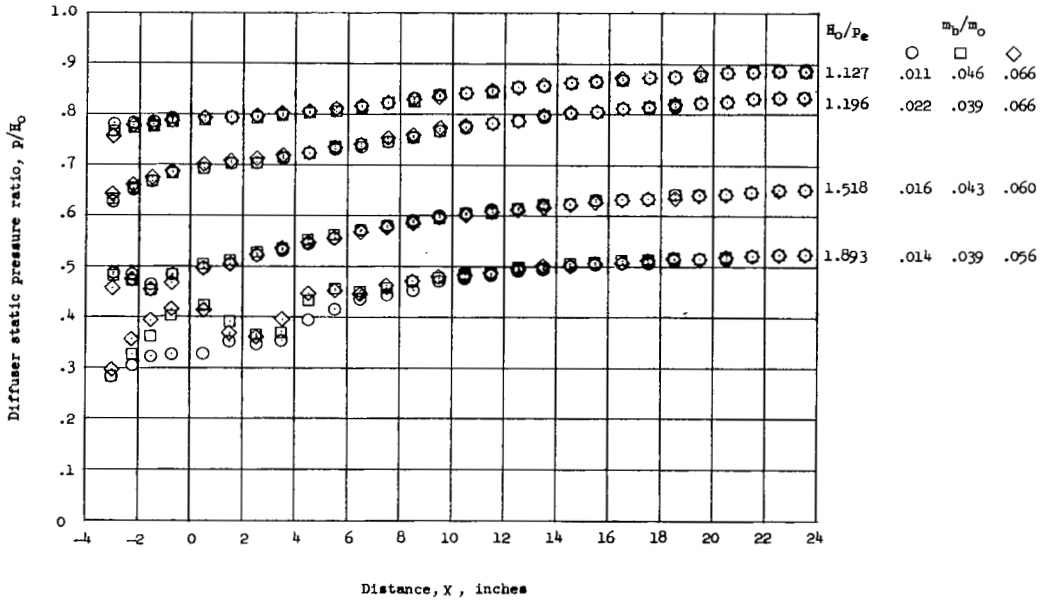

(e) Short shrouds. Diffuser II; $\delta_F = 10^\circ$; constant area mixing.

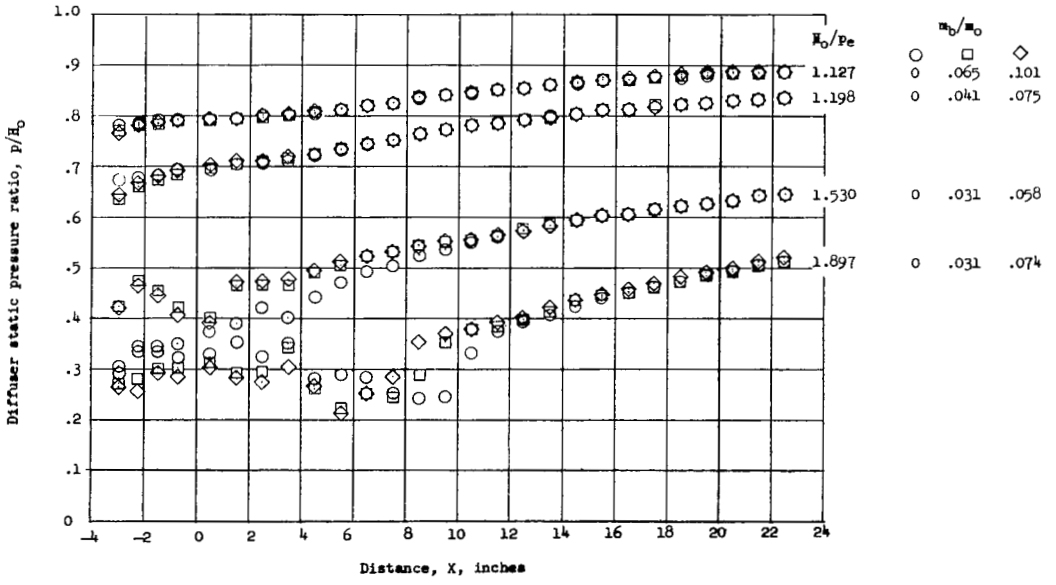

(f) Short shrouds. Diffuser III; $\delta_F = 10^\circ$; constant area mixing.

Figure 7.- Continued.

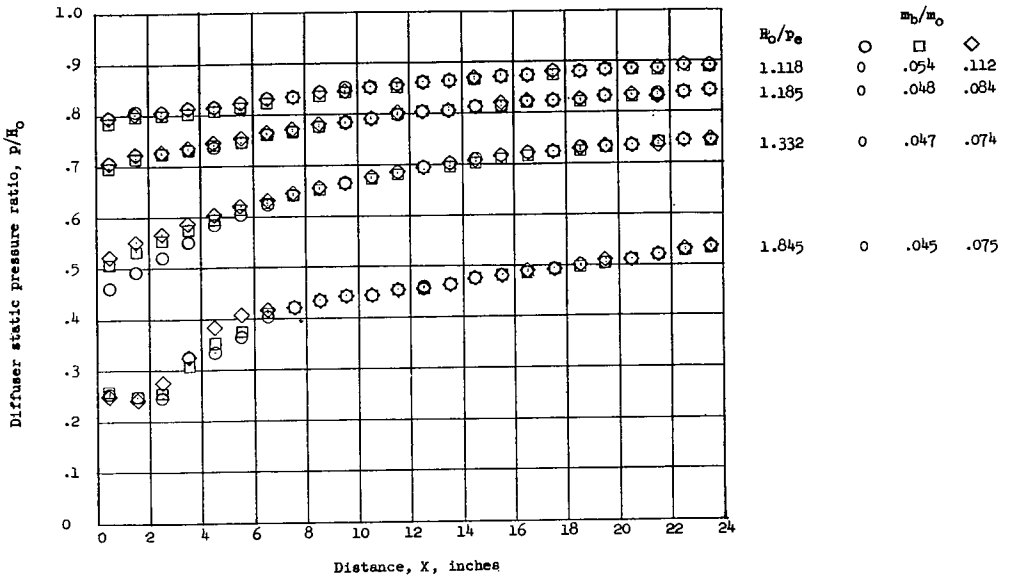

(g) Sharp-slot cutoff. Diffuser III; no flaps; fairing blocks in mixing section.

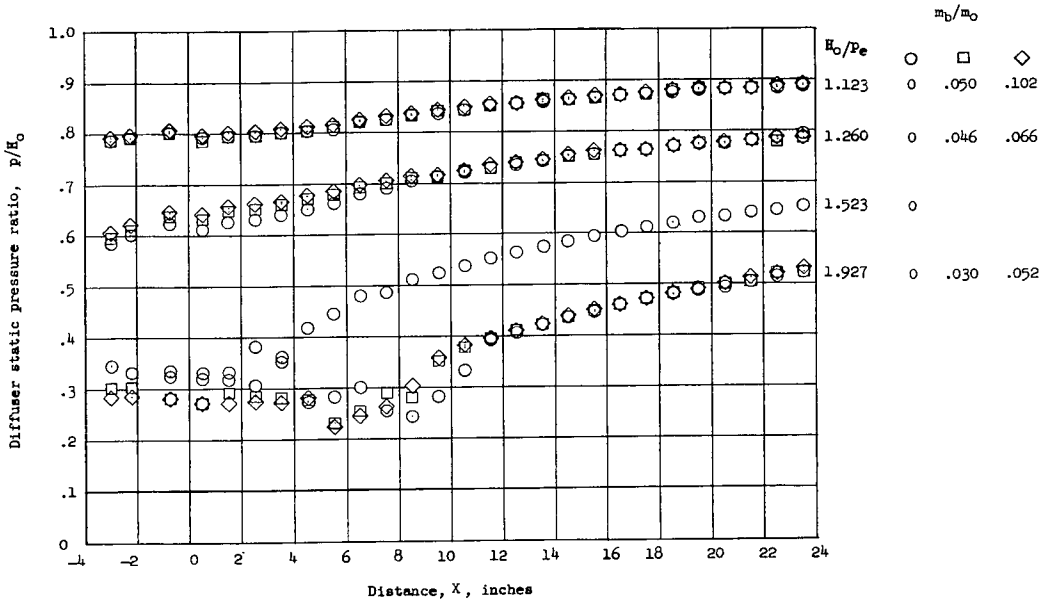

(h) Boattailed slots. Diffuser III; $\delta_F = 10^o$; constant area mixing.

Figure 7.- Continued.

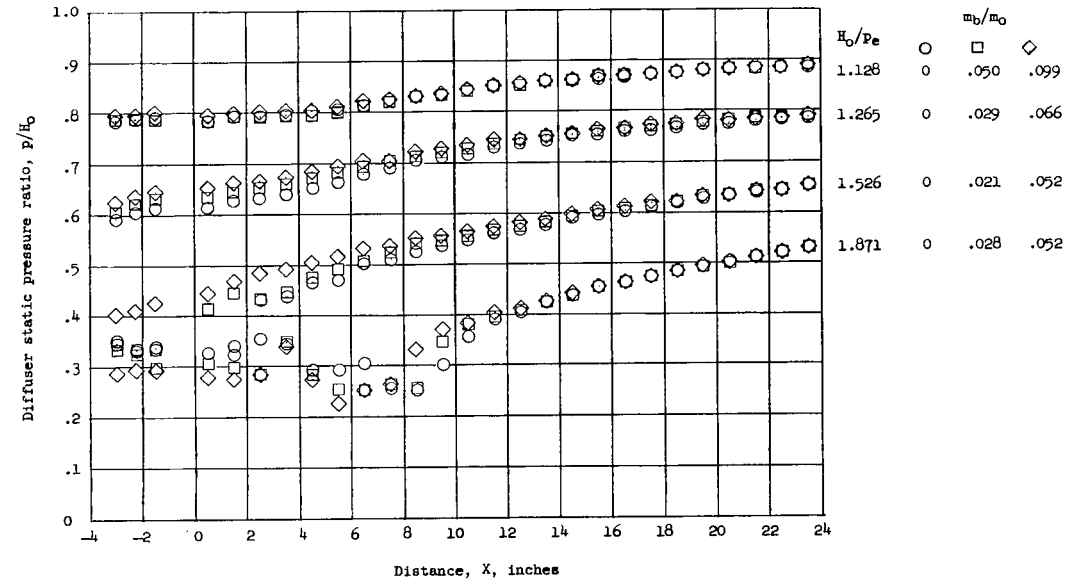

(i) Boattail flats removed. Diffuser III; $\delta_F = 10^o$; constant area mixing.

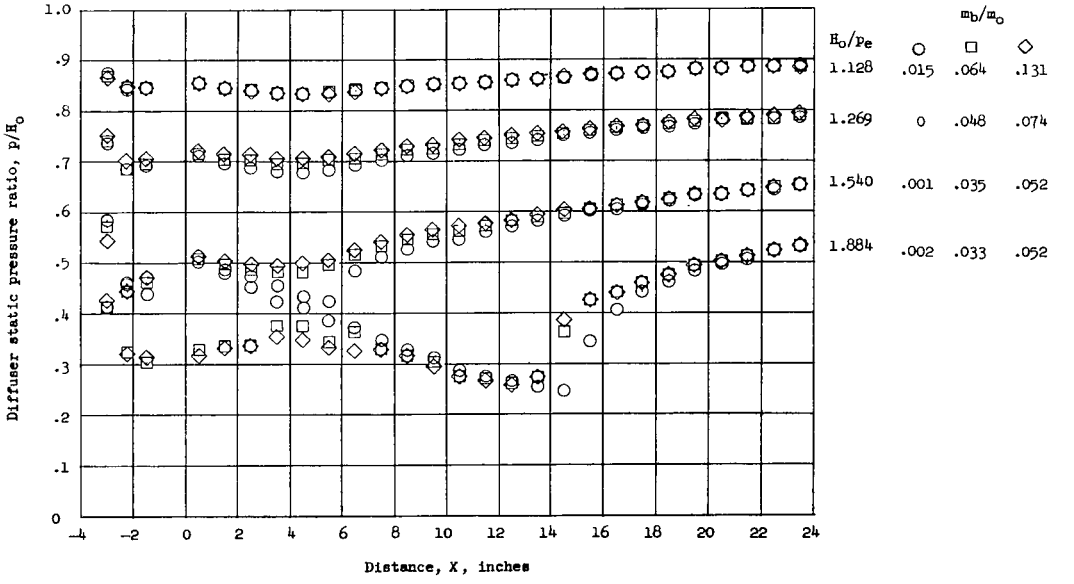

(j) Boattail flats removed. Diffuser IV; $\delta_F = 10^o$; constant area mixing.

Figure 7.- Continued.

[redacted]

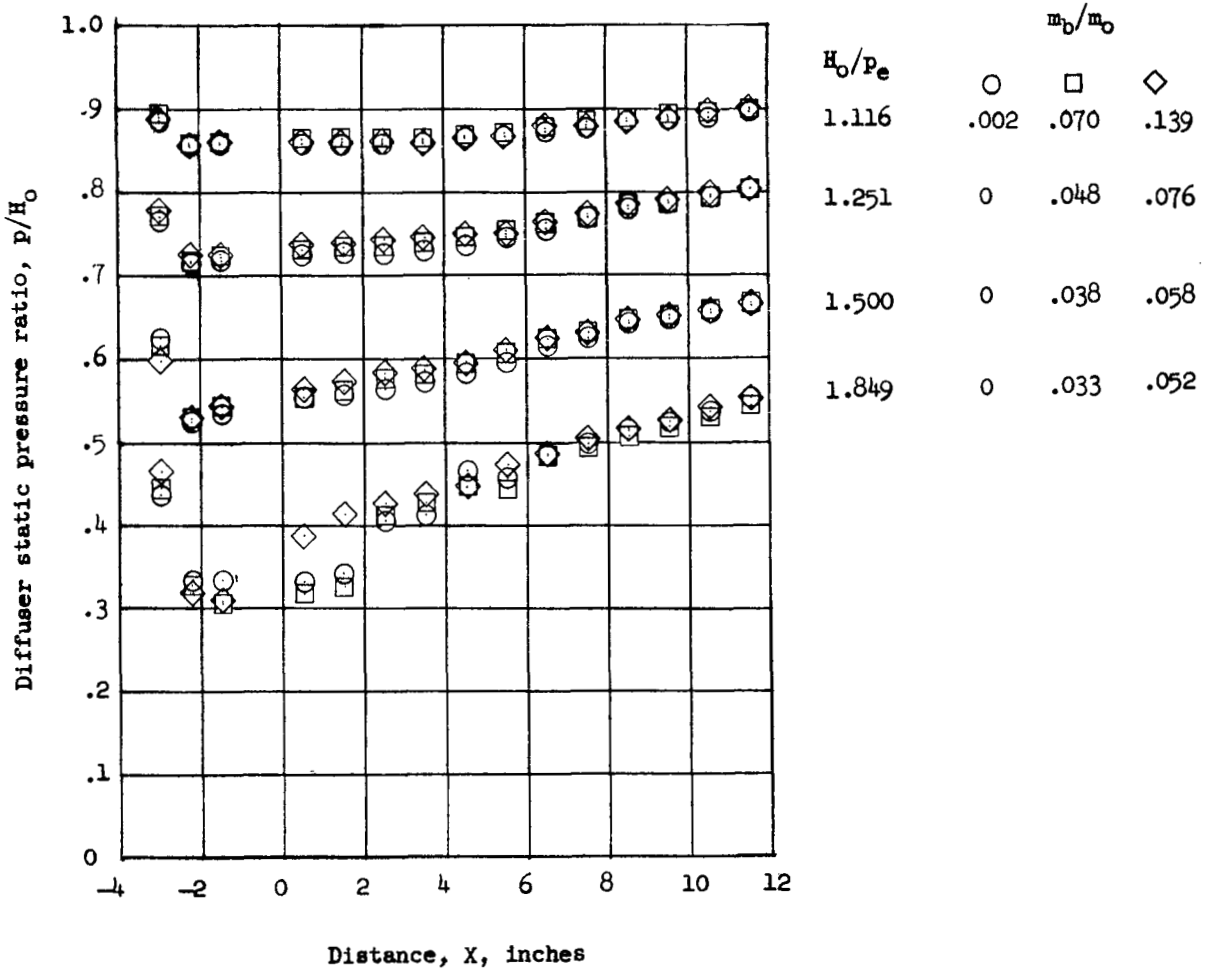

(k) Boattail flats removed. Diffuser V; $\delta_F = 10^o$; constant area mixing.

Figure 7.- Concluded.

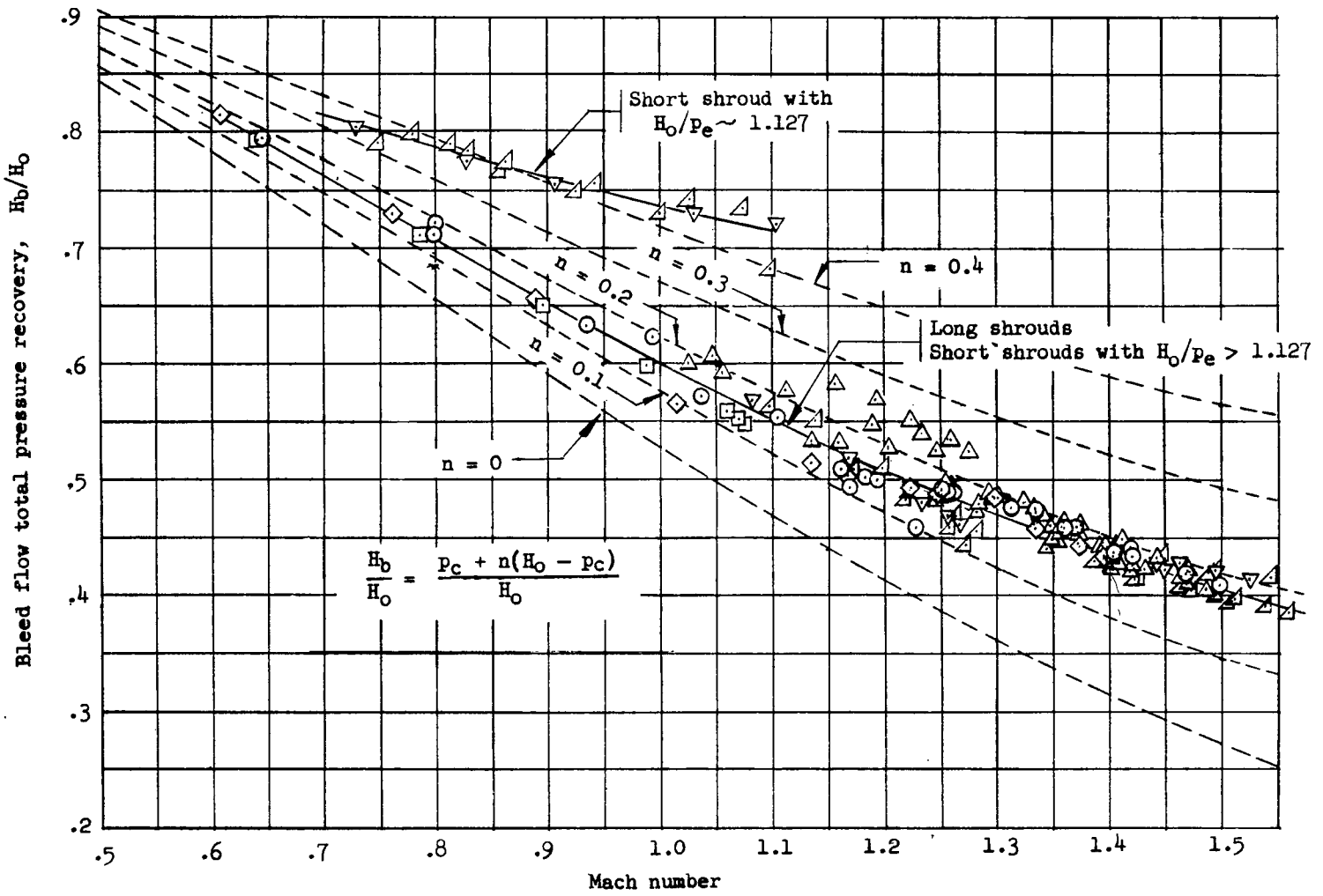

Figure 8.- Variation of bleed-flow total pressure recovery with Mach number.

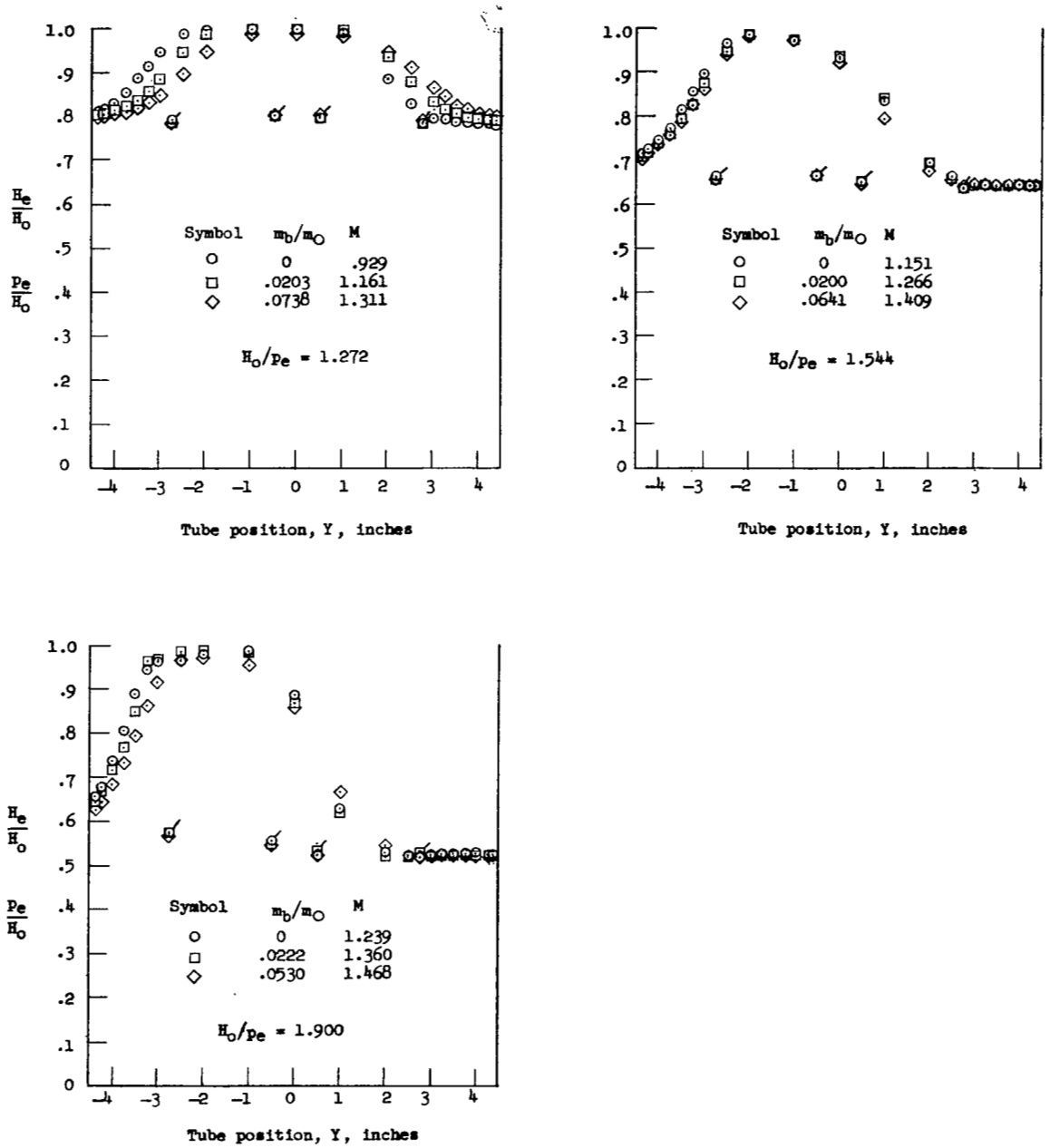

(a) Short shrouds with diffuser I. $\delta_F = 10^o$; rake in plane of expanding diffuser walls and slot flow. Flagged symbols indicate static pressures.

Figure 9.- Total and static pressure profiles measured at the diffuser exit.

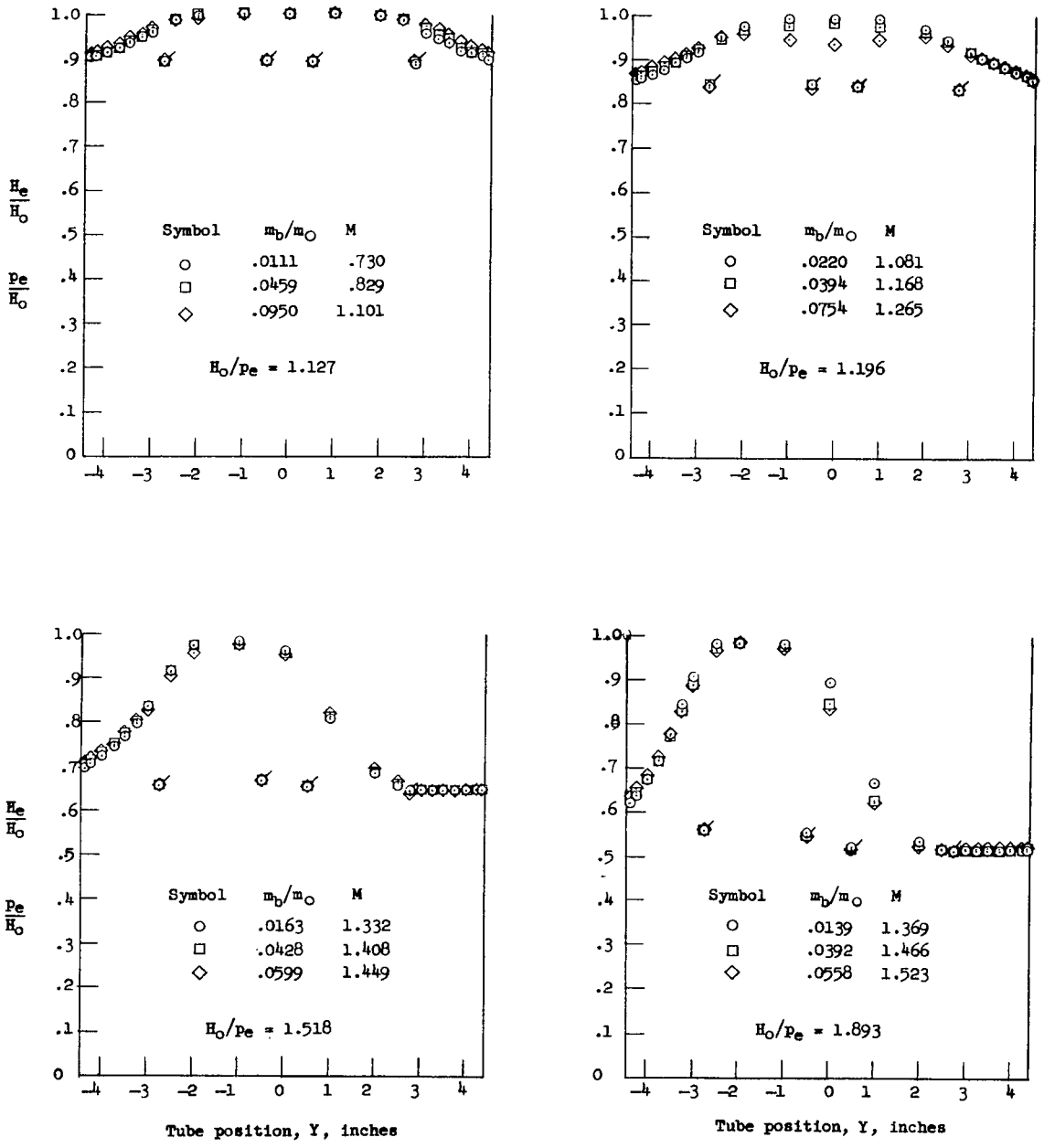

(b) Short shrouds with diffuser II. $\delta_F = 10^\circ$; rake in plane of expanding diffuser walls and slot flow. Flagged symbols indicate static pressures.

Figure 9.- Continued.

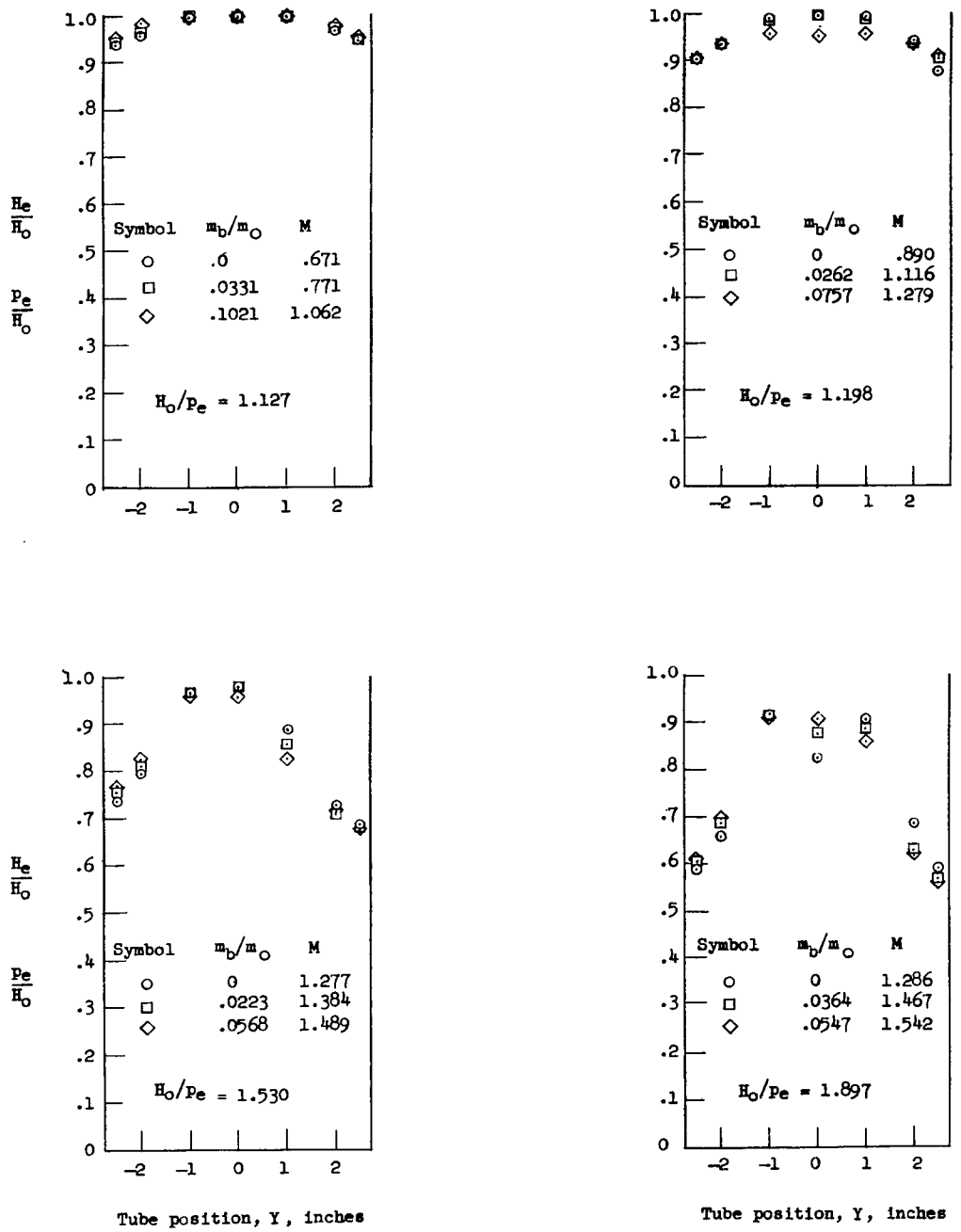

(c) Short shrouds with diffuser III. $\delta_F = 10^o$; rake in plane of slot flow.

Figure 9.- Continued.

[redacted]

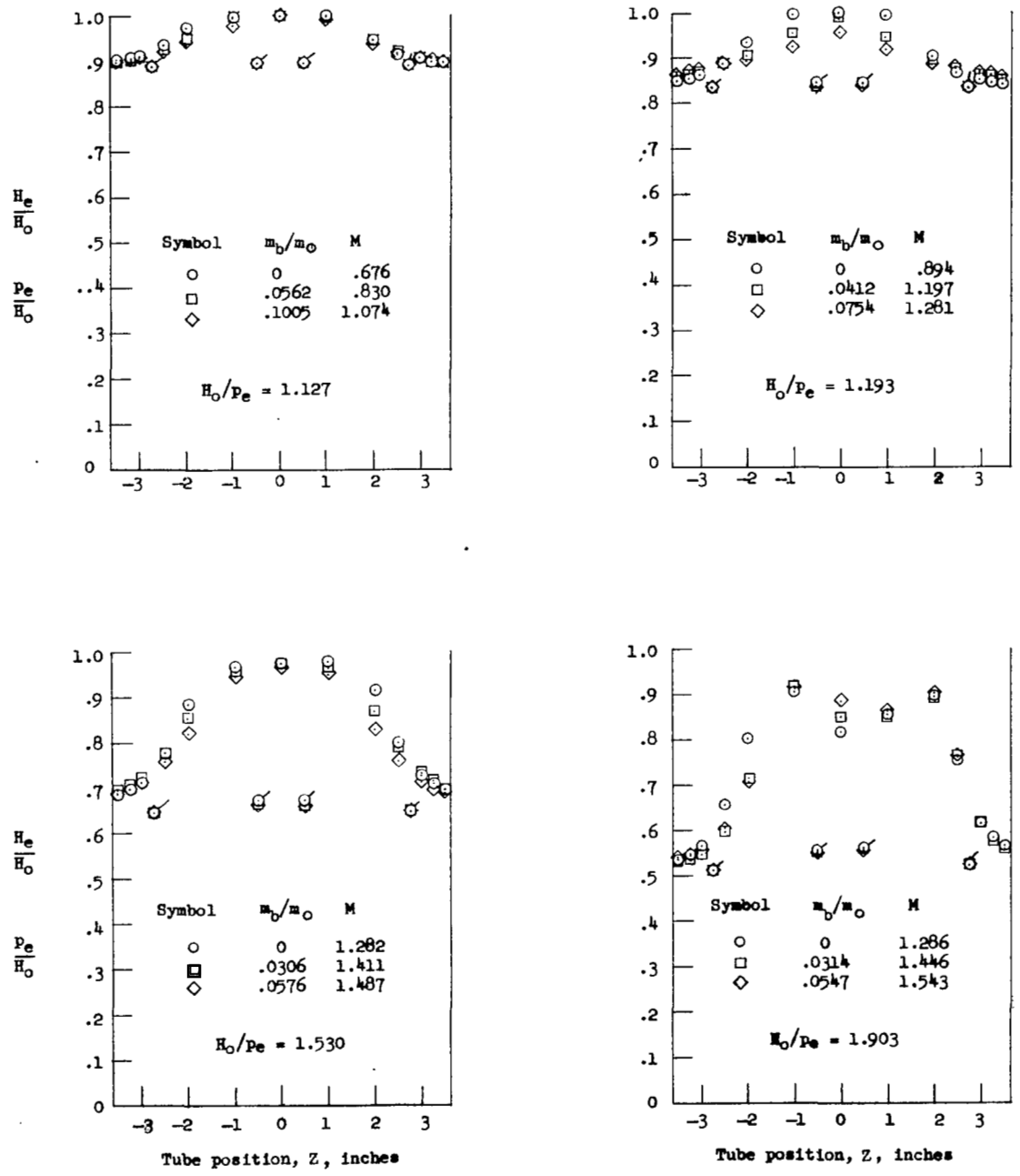

(d) Short shrouds with diffuser III. $\delta_F = 10^o$; rake in plane of expanding diffuser walls. Flagged symbols indicate static pressures.

Figure 9.- Continued.

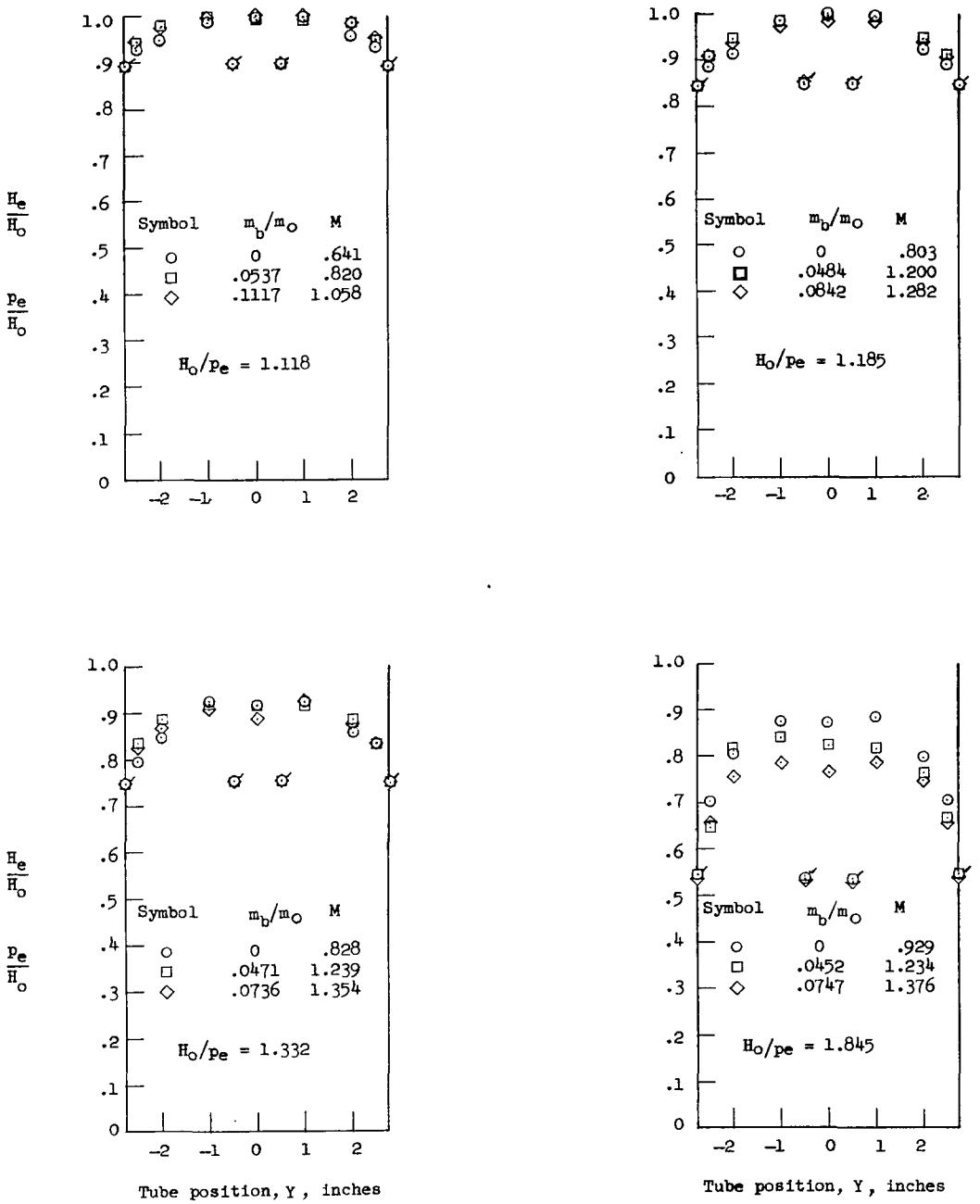

(e) Sharp-slot cutoff. Diffuser III; no flaps; rake vertical. Flagged symbols indicate static pressures.

Figure 9.- Continued.

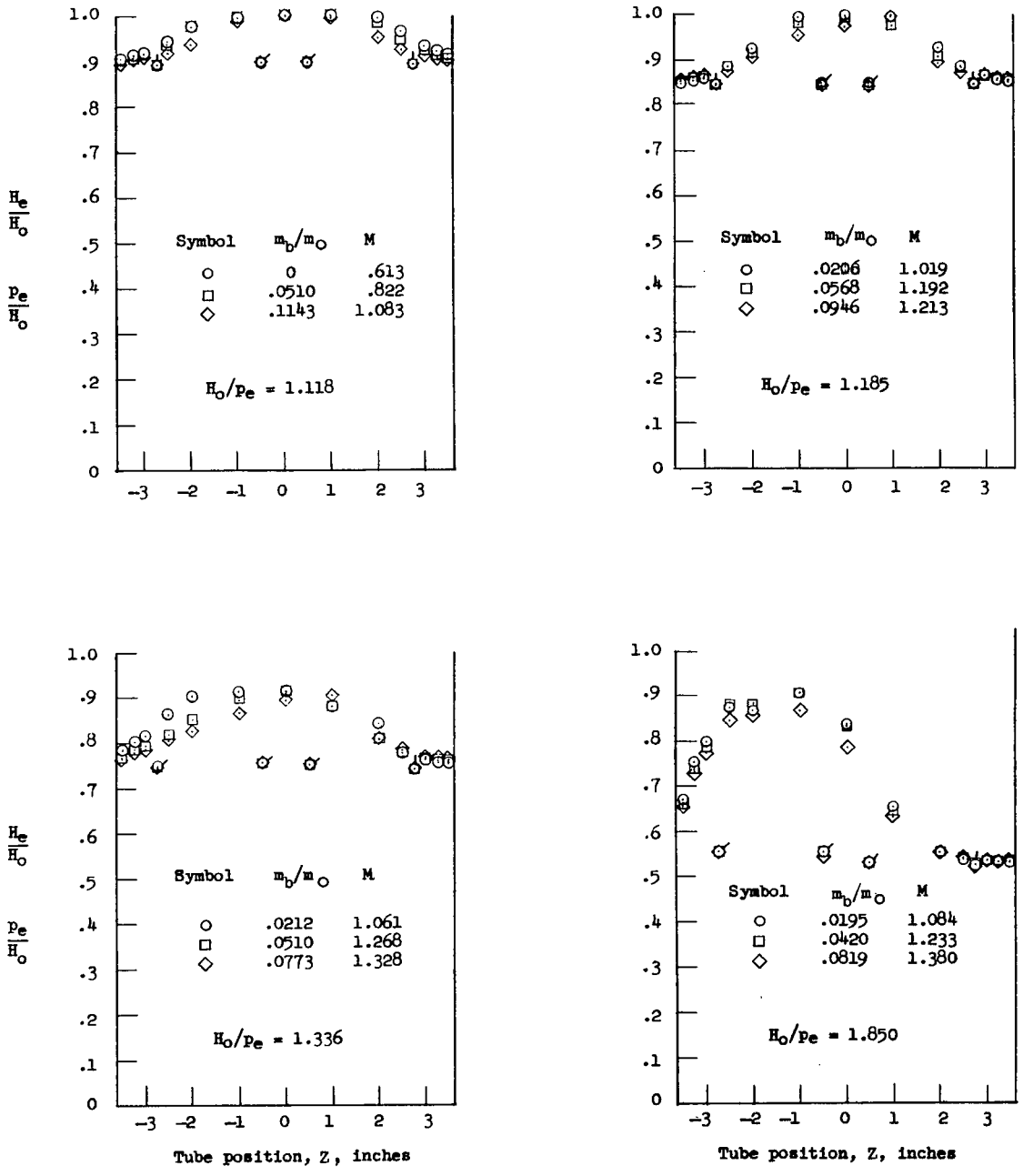

(f) Sharp-slot cutoff. Diffuser III; no flaps; rake in plane of expanding diffuser walls. Flagged symbols indicate static pressures.

Figure 9.- Continued.

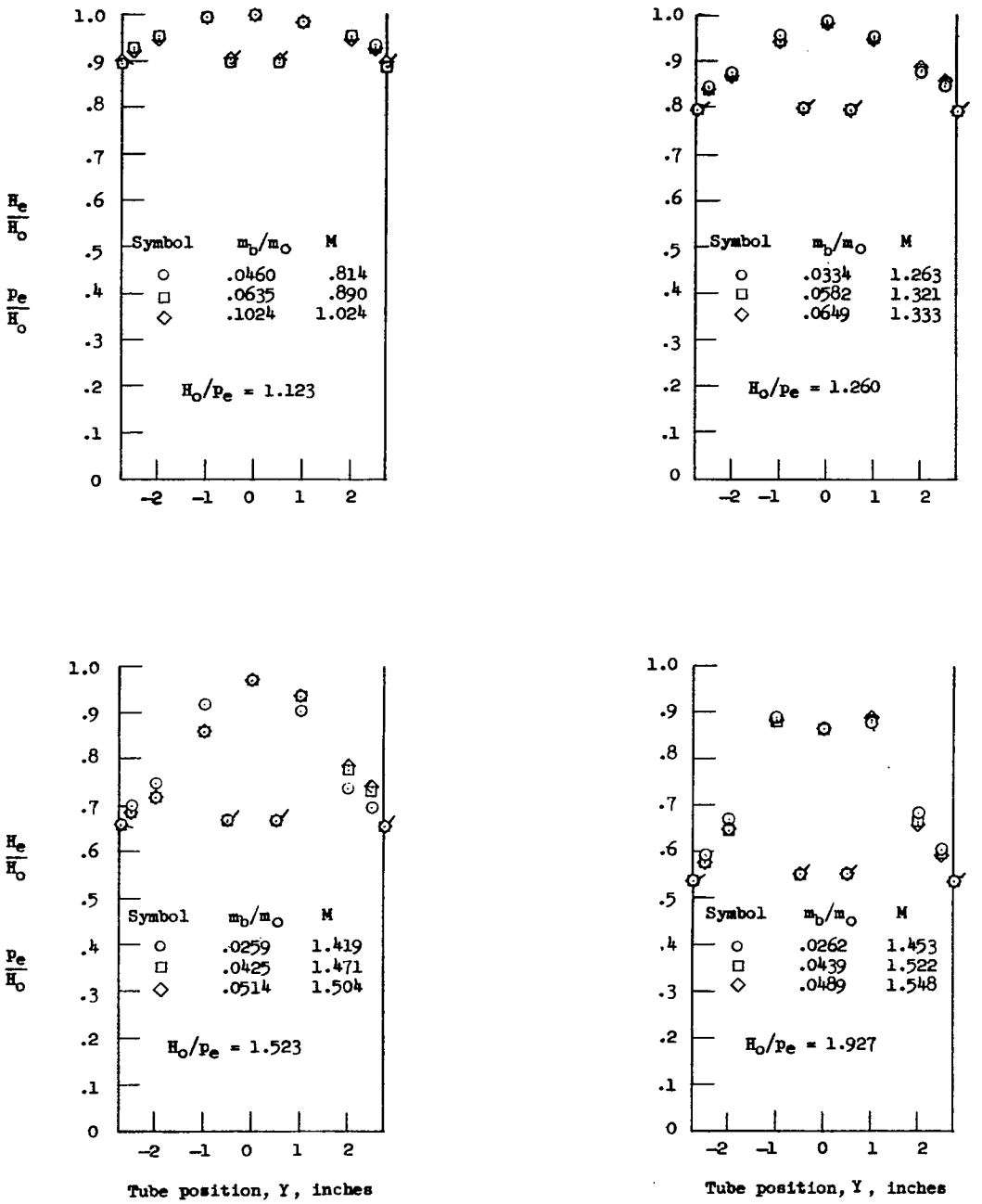

(g) Boattails. Diffuser III; $\delta_F = 10^\circ$; rake in plane of slot flow. Flagged symbols indicate static pressures.

Figure 9.- Continued.

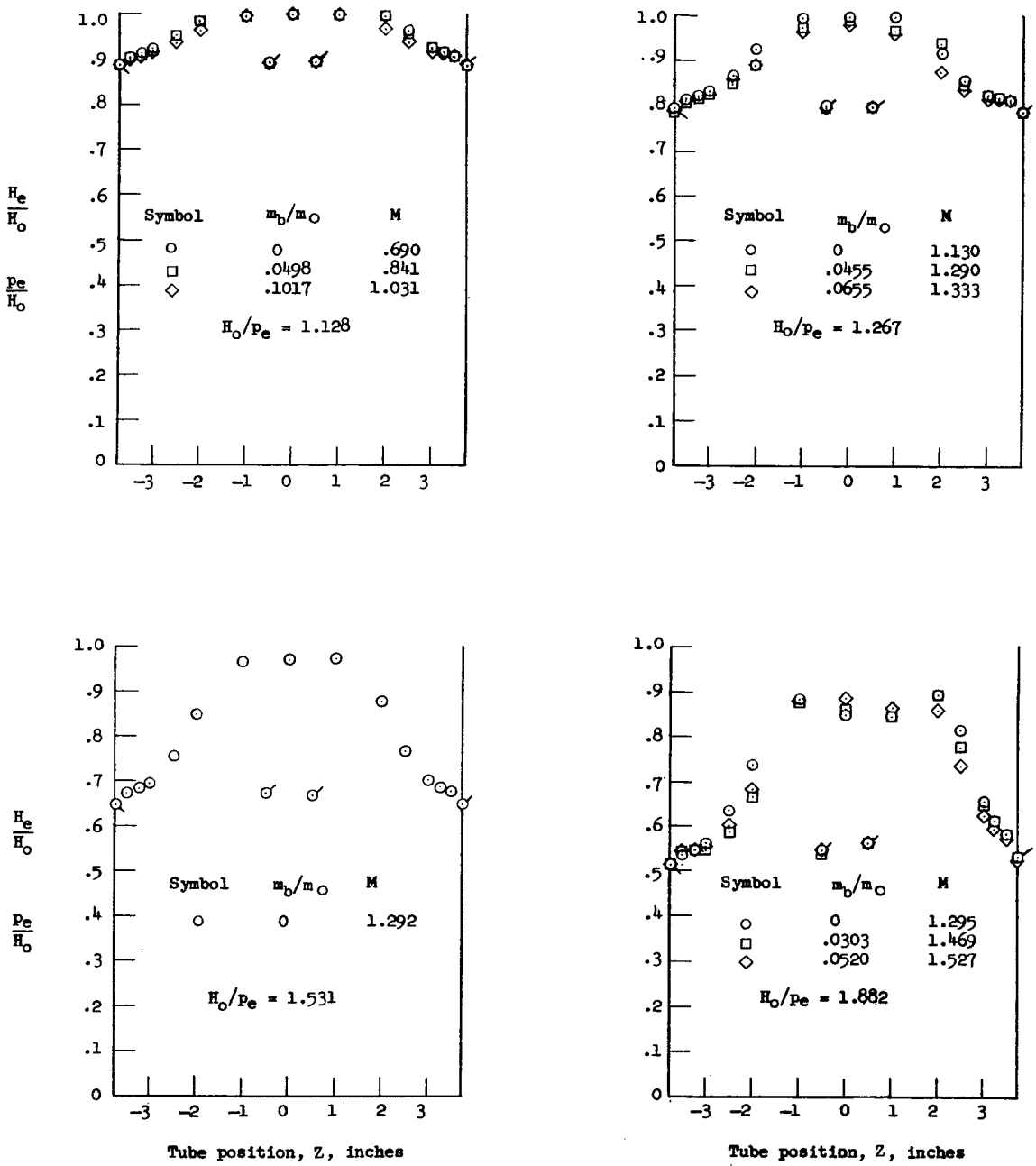

(h) Boattails. Diffuser III; $\delta_F = 10^\circ$; rake in plane of expanding diffuser walls. Flagged symbols indicate static pressures.

Figure 9.- Continued.

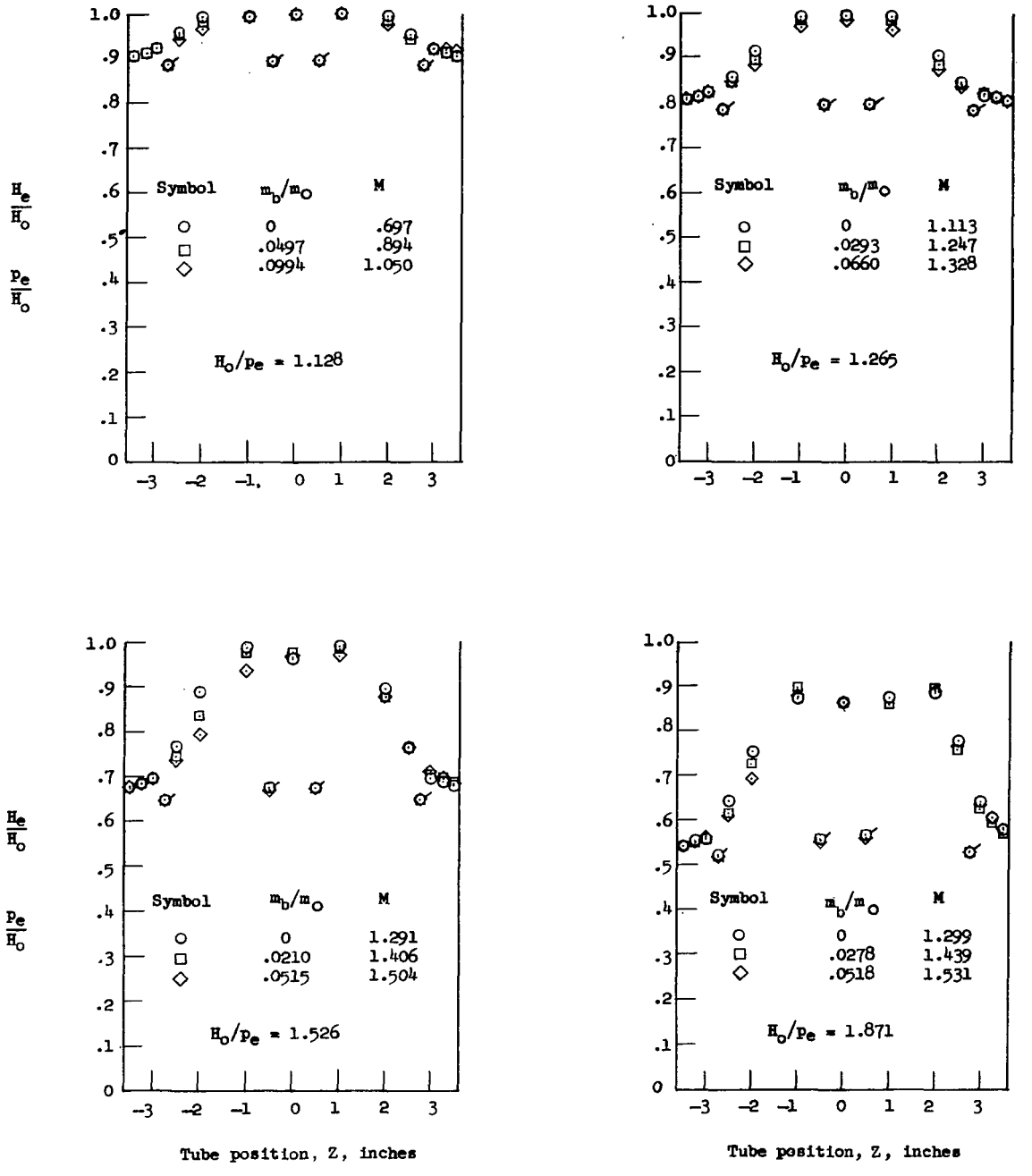

(i) Boattail flats removed. Diffuser III; $\delta_F = 10^\circ$; rake in plane of expanding diffuser walls. Flagged symbols indicate static pressures.

Figure 9.- Continued.

[redacted]

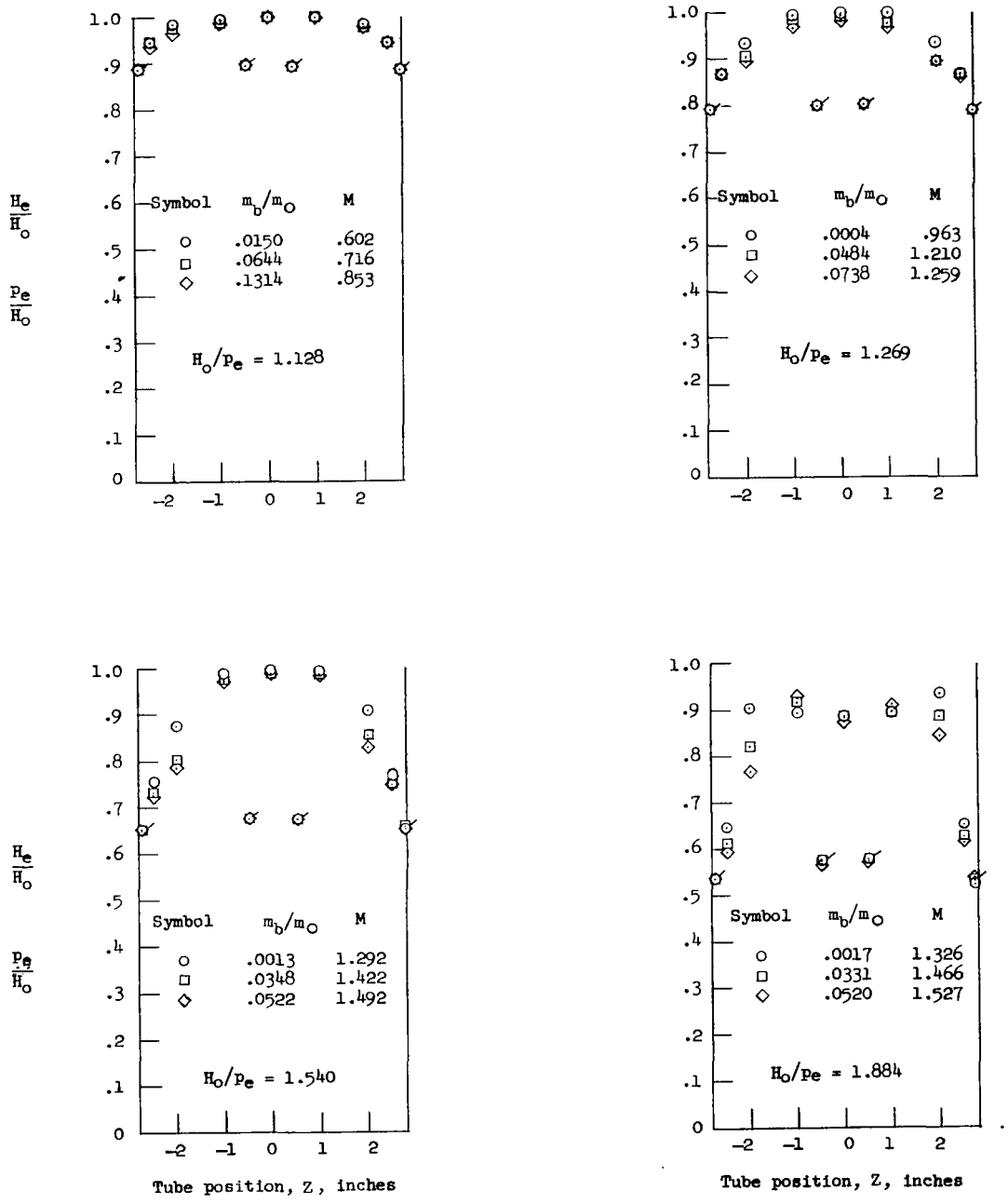

(j) Boattail flats removed. Diffuser IV; $\delta_F = 10^o$; rake in plane of expanding diffuser walls. Flagged symbols indicate static pressures.

Figure 9.- Continued.

[redacted]

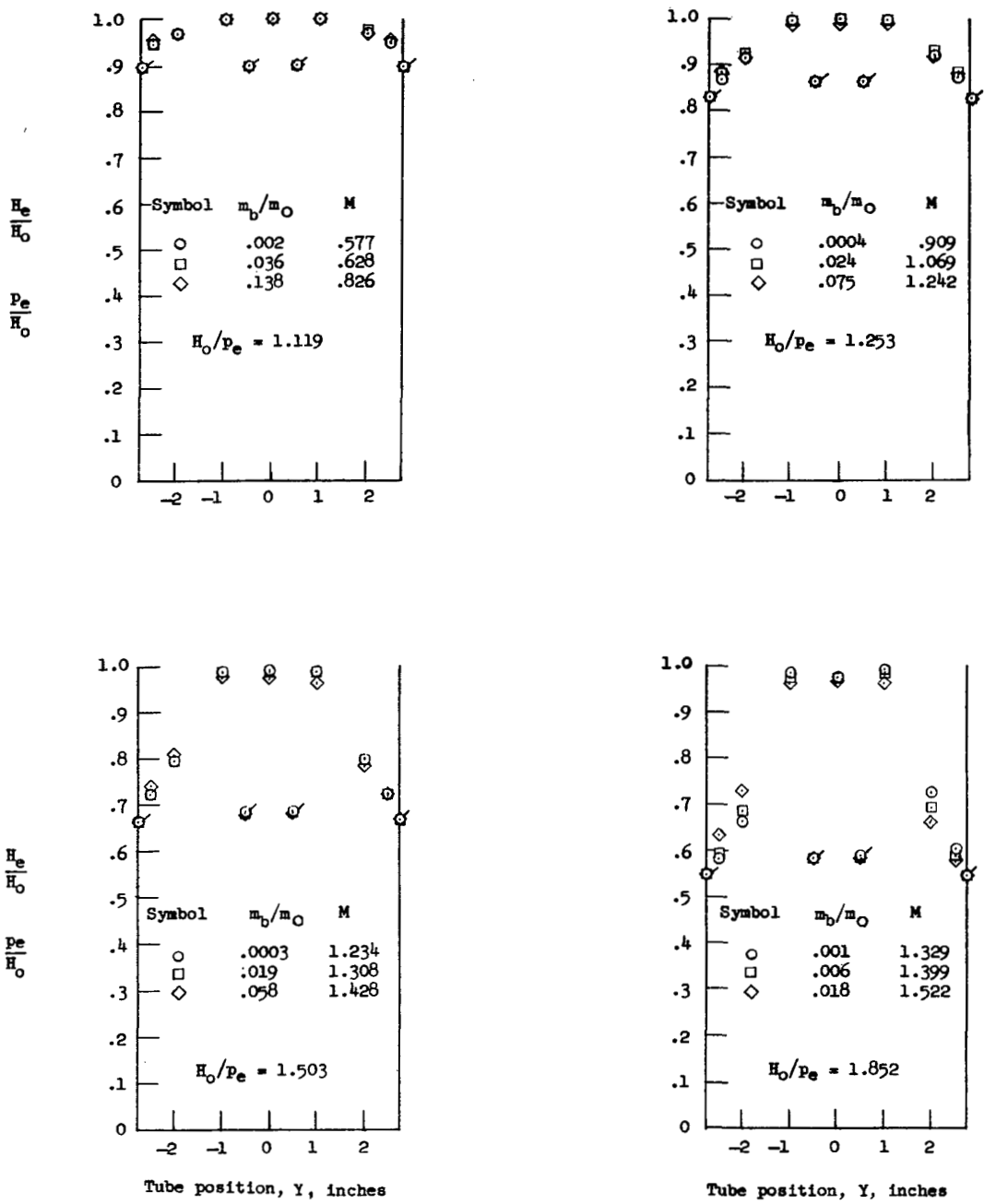

(k) Boattail flats removed. Diffuser V; $\delta_F = 10^\circ$; rake in plane of slot flow. Flagged symbols indicate static pressures.

Figure 9.- Continued.

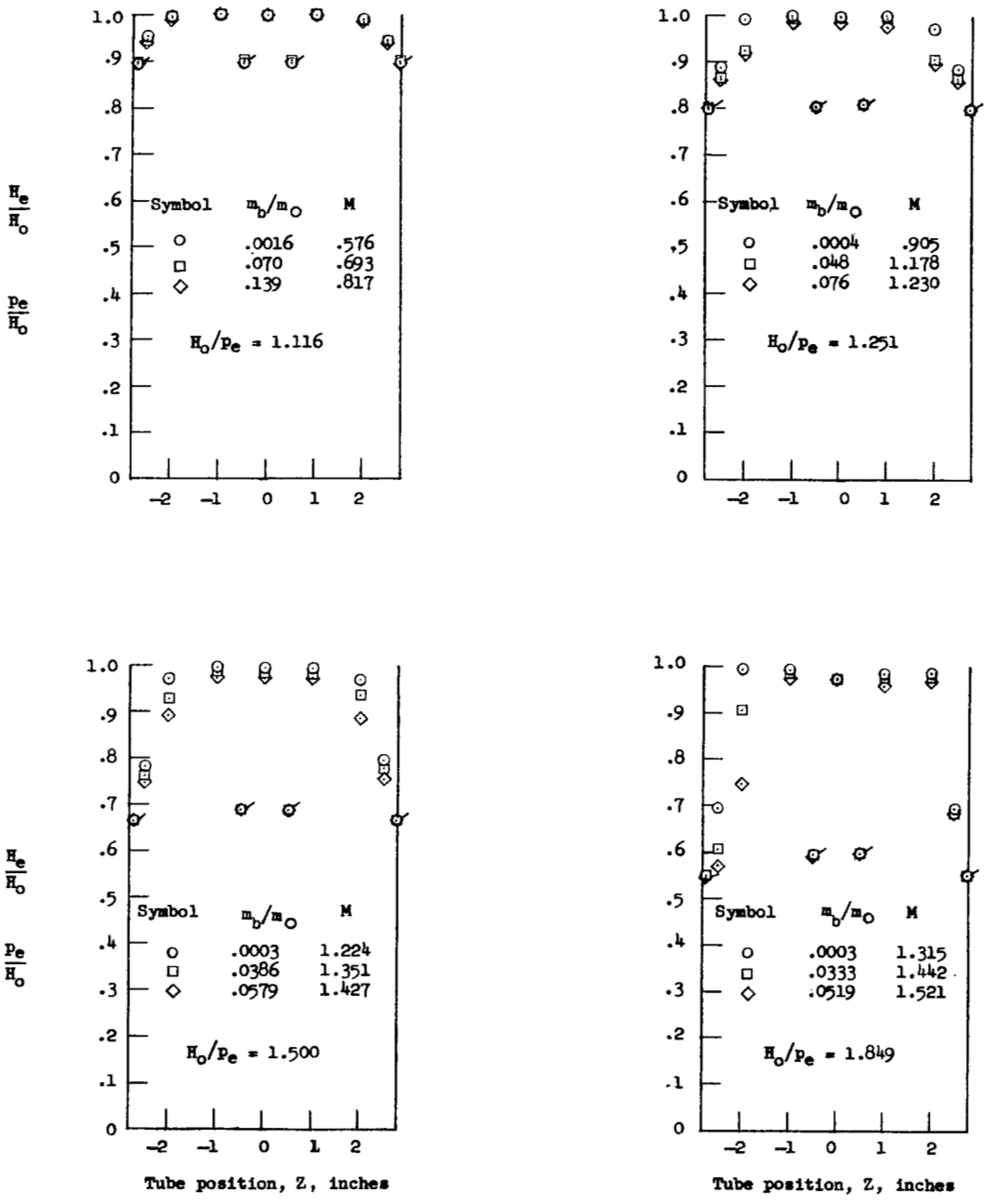

(l) Boattail flats removed. Diffuser V; $\delta_F = 10^\circ$; rake in plane of expanding diffuser walls. Flagged symbols indicate static pressures.

Figure 9.- Concluded.

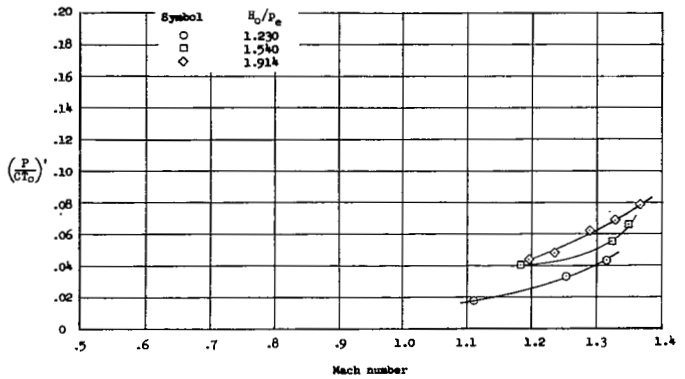

(a) Short shrouds and diffuser I. $\delta_F = 0^\circ$.

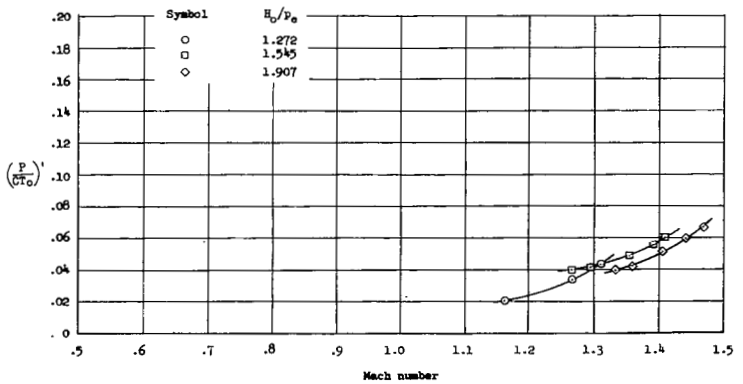

(b) Short shrouds and diffuser I. $\delta_F = 10^\circ$.

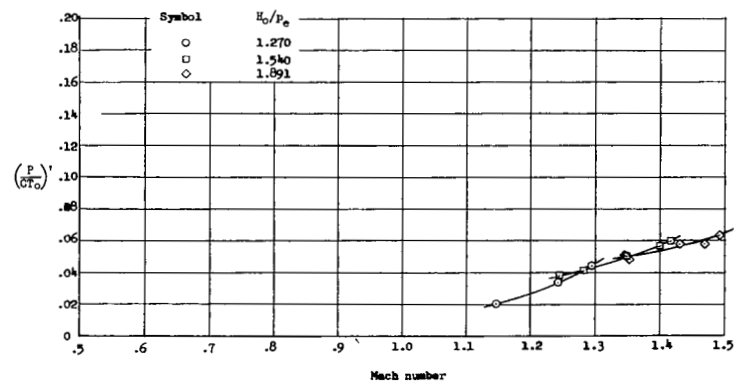

(c) Short shrouds and diffuser I. $\delta_F = 20^\circ$.

Figure 10.- Variation of power coefficient with Mach number for several values of tunnel pressure ratio. Diffuser exit rake vertical.

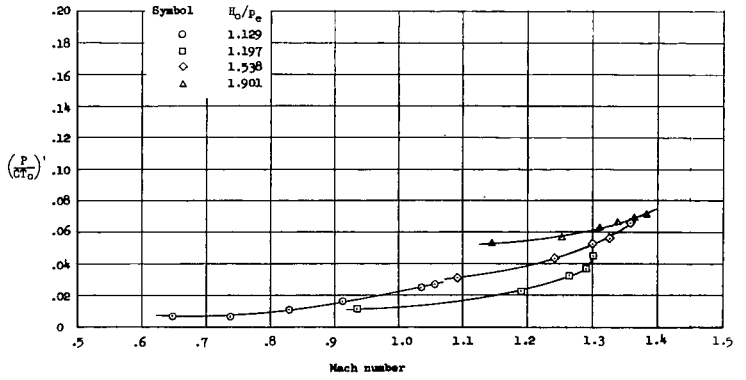

(d) Short shrouds and diffuser II. $\delta_F = 0^\circ$.

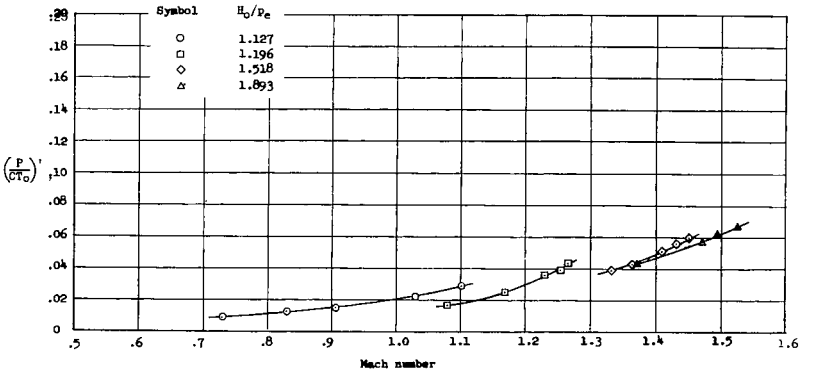

(e) Short shrouds and diffuser II. $\delta_F = 10^\circ$.

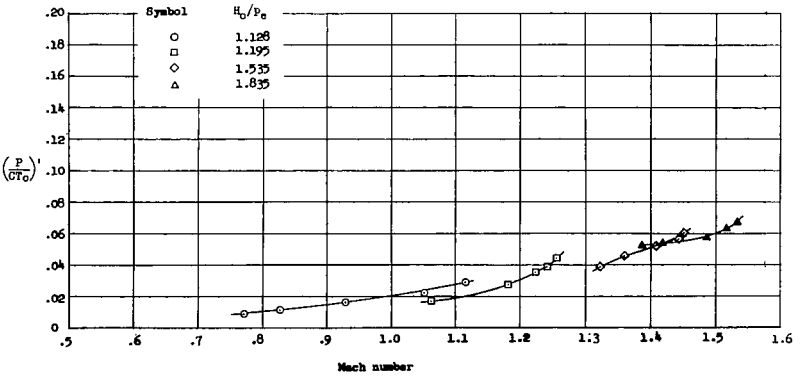

(f) Short shrouds and diffuser II. $\delta_F = 20^\circ$.

Figure 10.- Concluded.

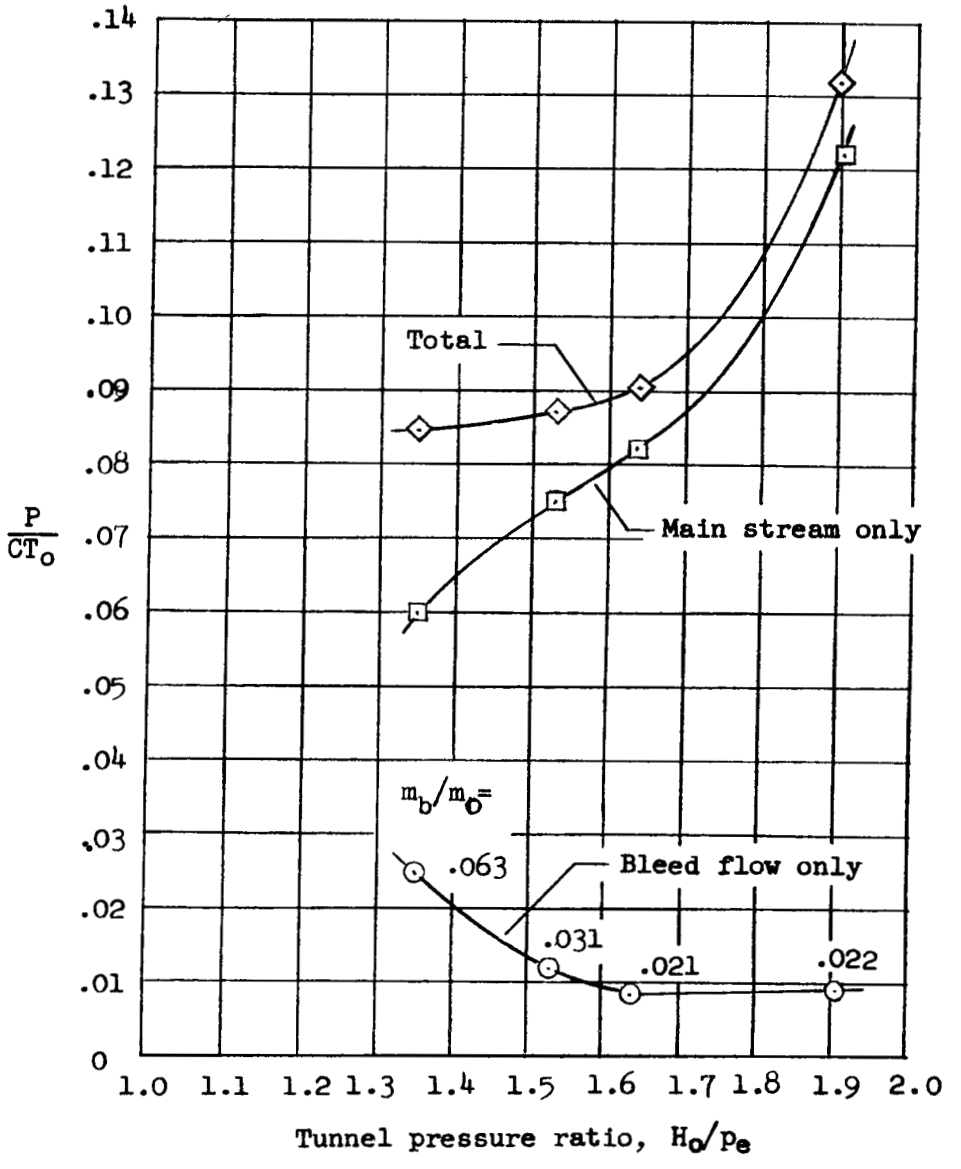

Figure 11.- Variation of power with tunnel pressure ratio. Bleed-flow rate varied to maintain the Mach number constant at 1.41.

[redacted]

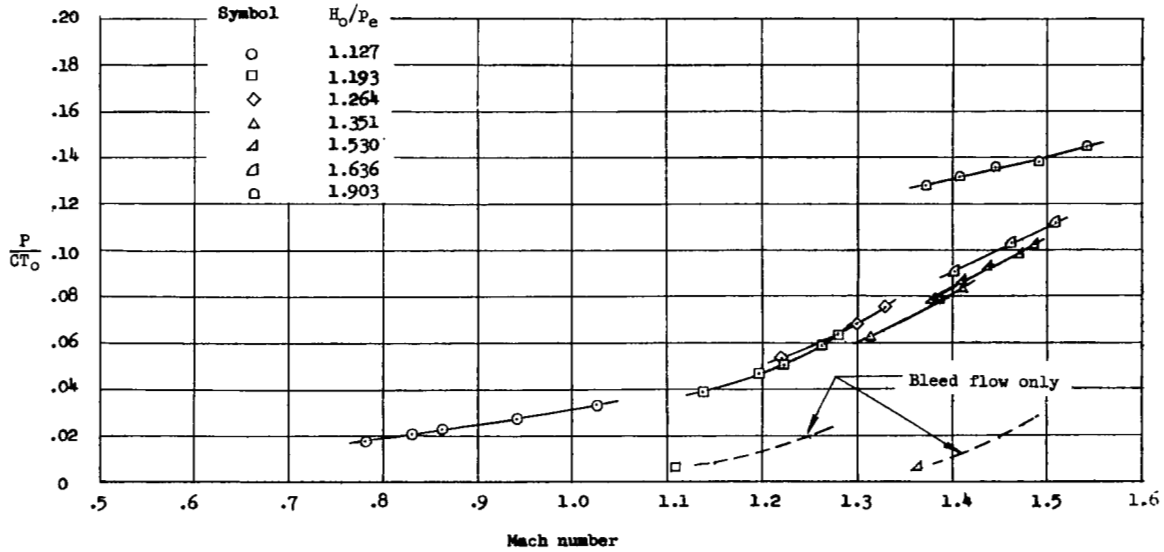

(a) Short shrouds and diffuser III. $\delta_F = 10^o$.

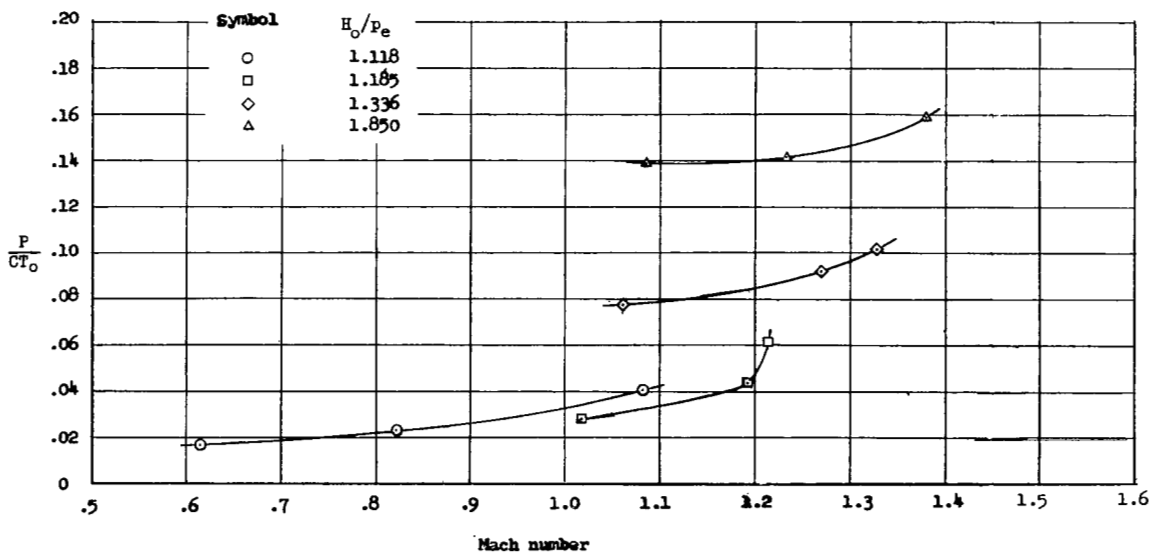

(b) Sharp-slot cutoff without flaps. Diffuser III faired through mixing section to surface of slotted floor.

Figure 12.- Variation of power coefficient with Mach number for several values of tunnel pressure ratio. Diffuser exit rakes vertical and horizontal.

[redacted]

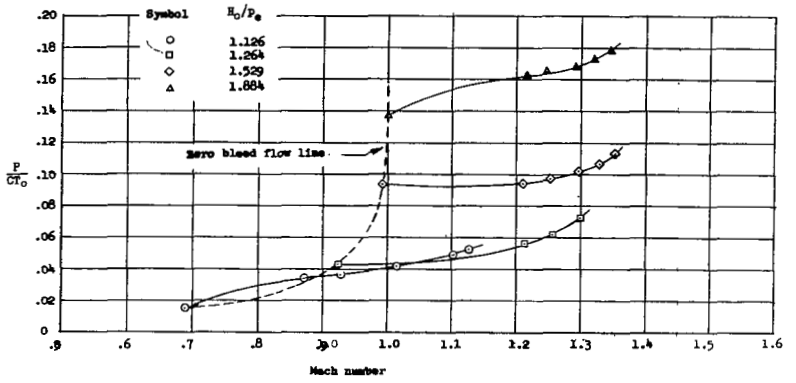

(c) Boattailed slots with diffuser III. $\delta_F = 0^\circ$.

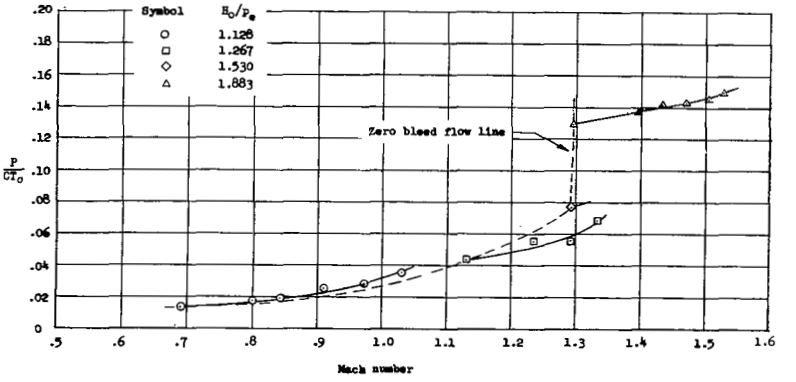

(d) Boattailed slots with diffuser III. $\delta_F = 10^\circ$.

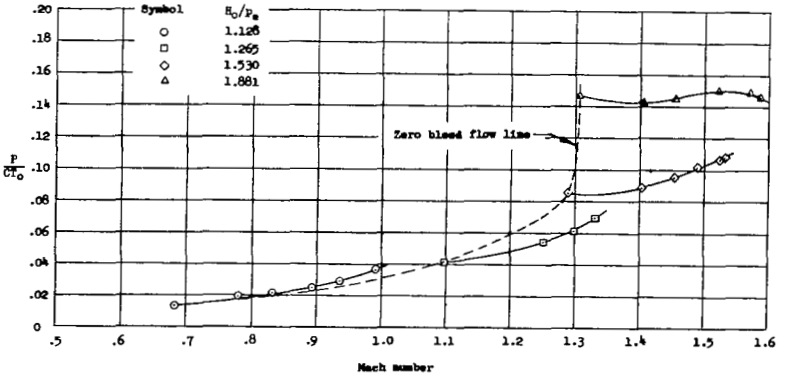

(e) Boattailed slots with diffuser III. $\delta_F = 20^\circ$.

Figure 12.- Continued.

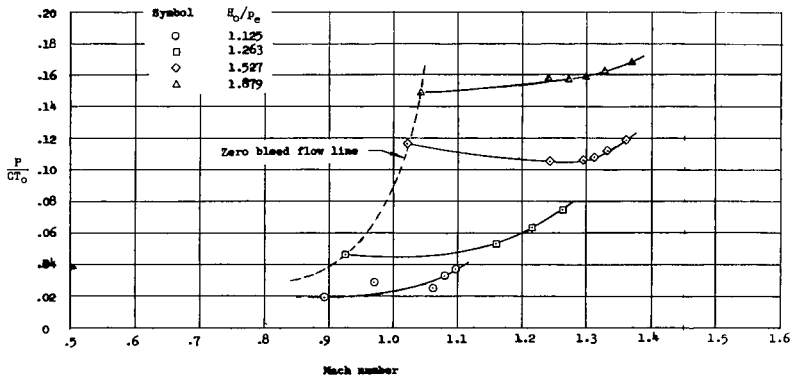

(f) Flats removed from boattail region. Diffuser III; $\delta_F = 0^\circ$.

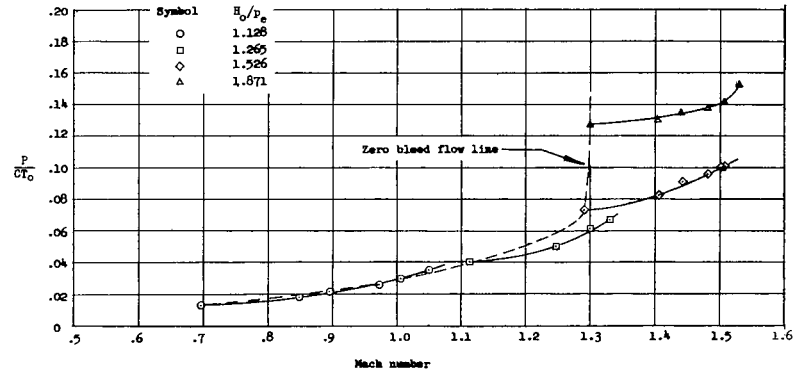

(g) Flats removed from boattail region. Diffuser III; $\delta_F = 10^\circ$.

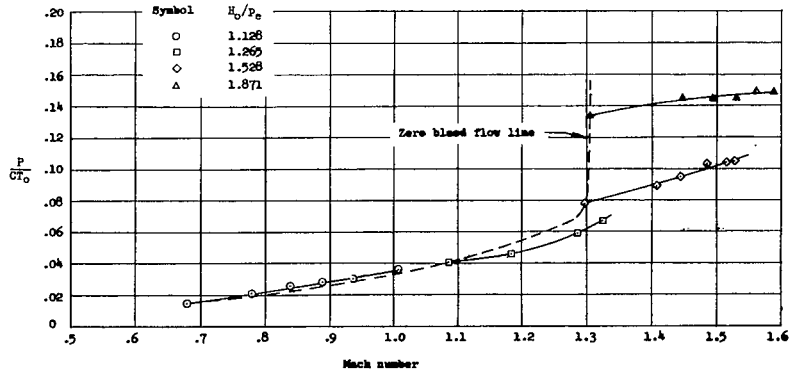

(h) Flats removed from boattail region. Diffuser III; $\delta_F = 20^\circ$.

Figure 12.- Continued.

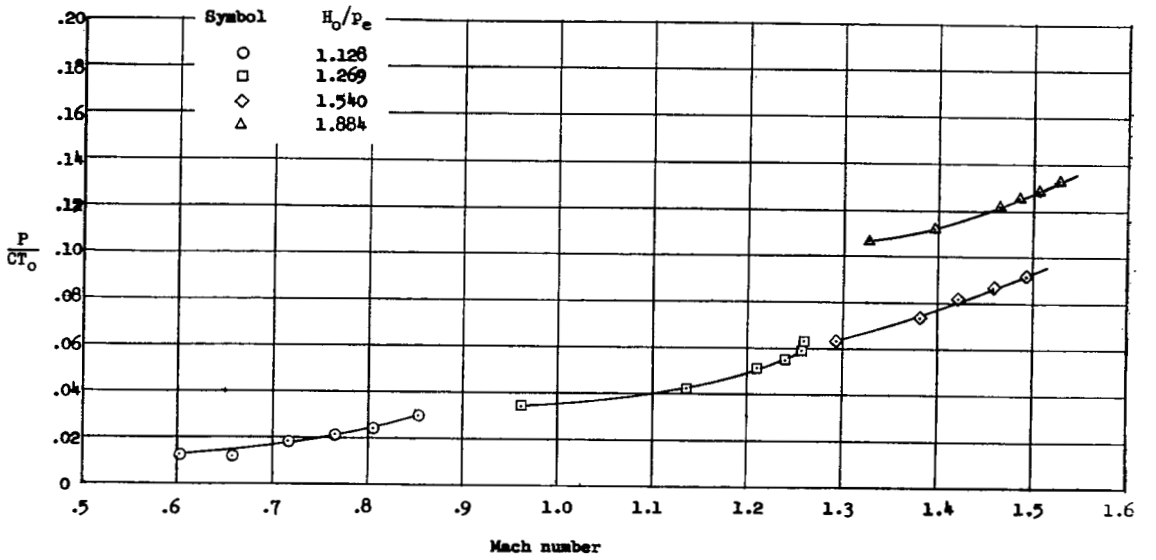

(i) Flats removed from boattail region. Diffuser IV; $\delta_F = 10^\circ$.

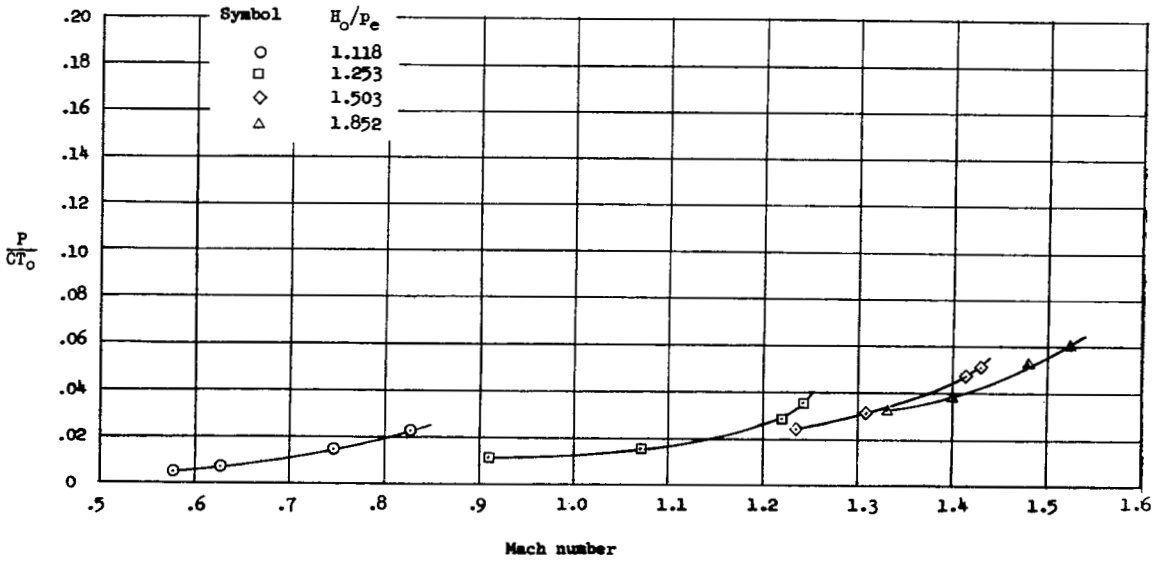

(j) Flats removed from boattail region. Diffuser V; $\delta_F = 10^\circ$.

Figure 12.- Concluded.

[redacted]

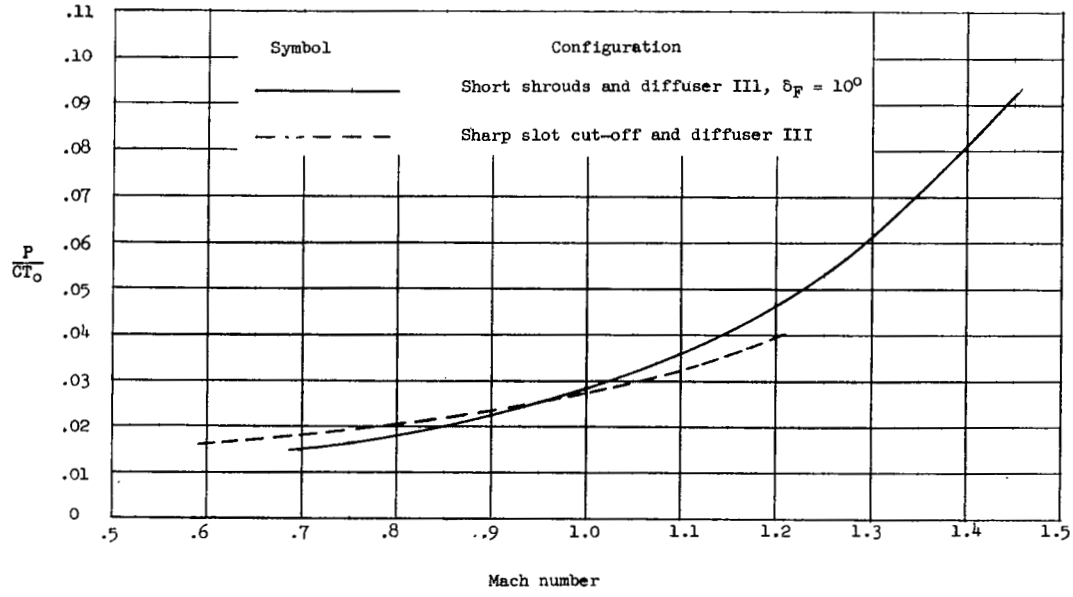

(a) Short shrouds and sharp-slot cutoff.

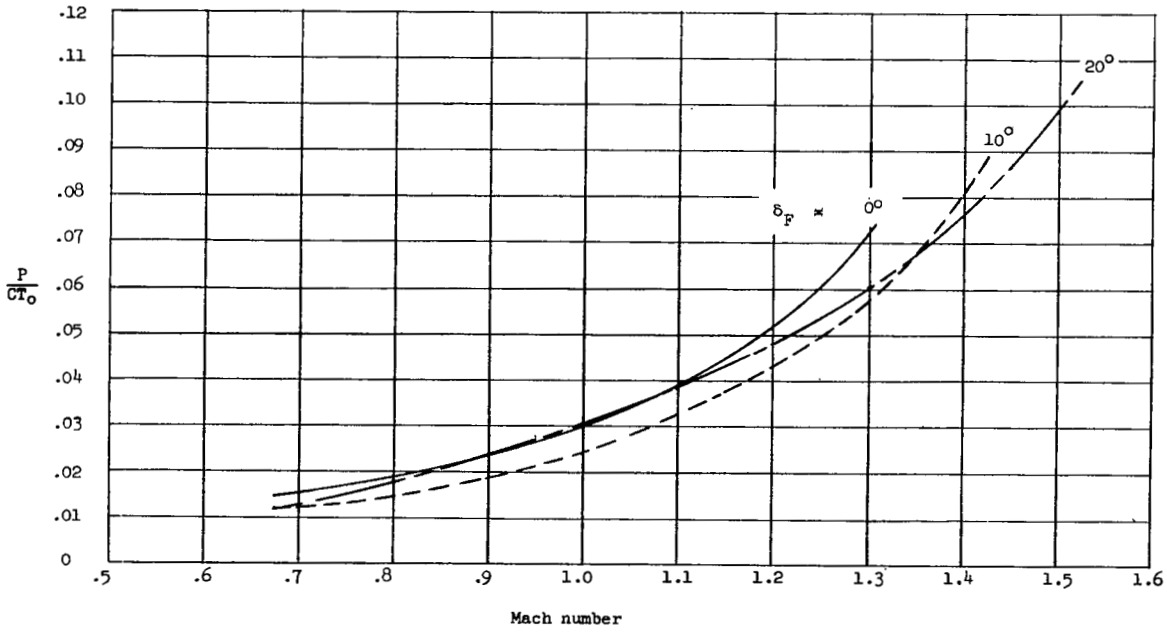

(b) Boattail floor bars with diffuser III.

Figure 13.- Envelope curves of the variation of power required with Mach number.

[redacted]

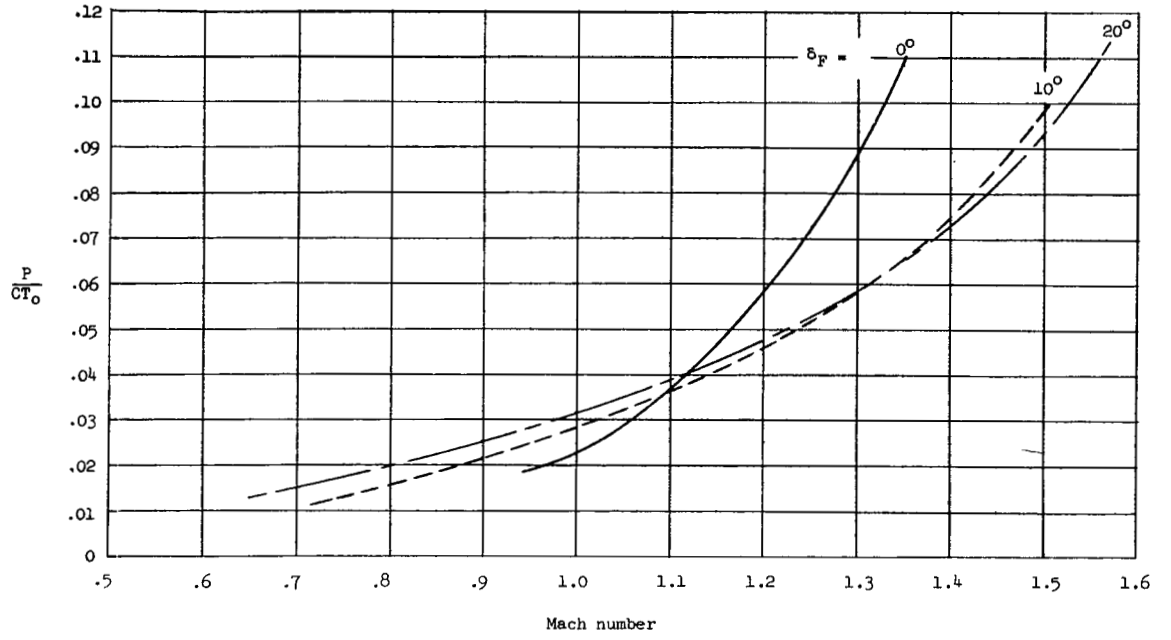

(c) Flats removed from boattail region. Diffuser III.

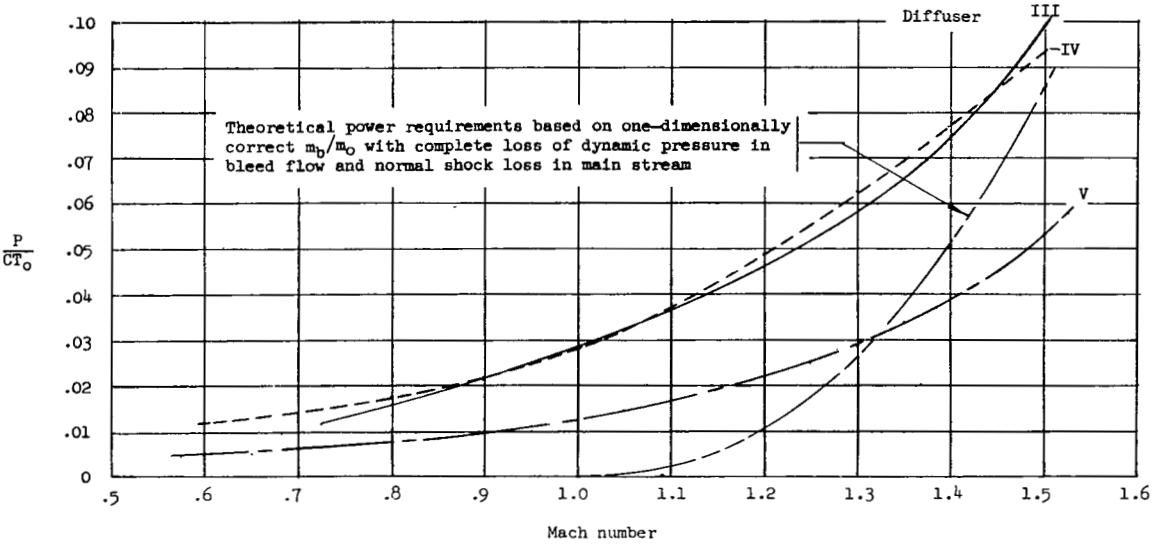

(d) Flats removed from boattail region. $\delta_F = 10^o$.

Figure 13.- Concluded.

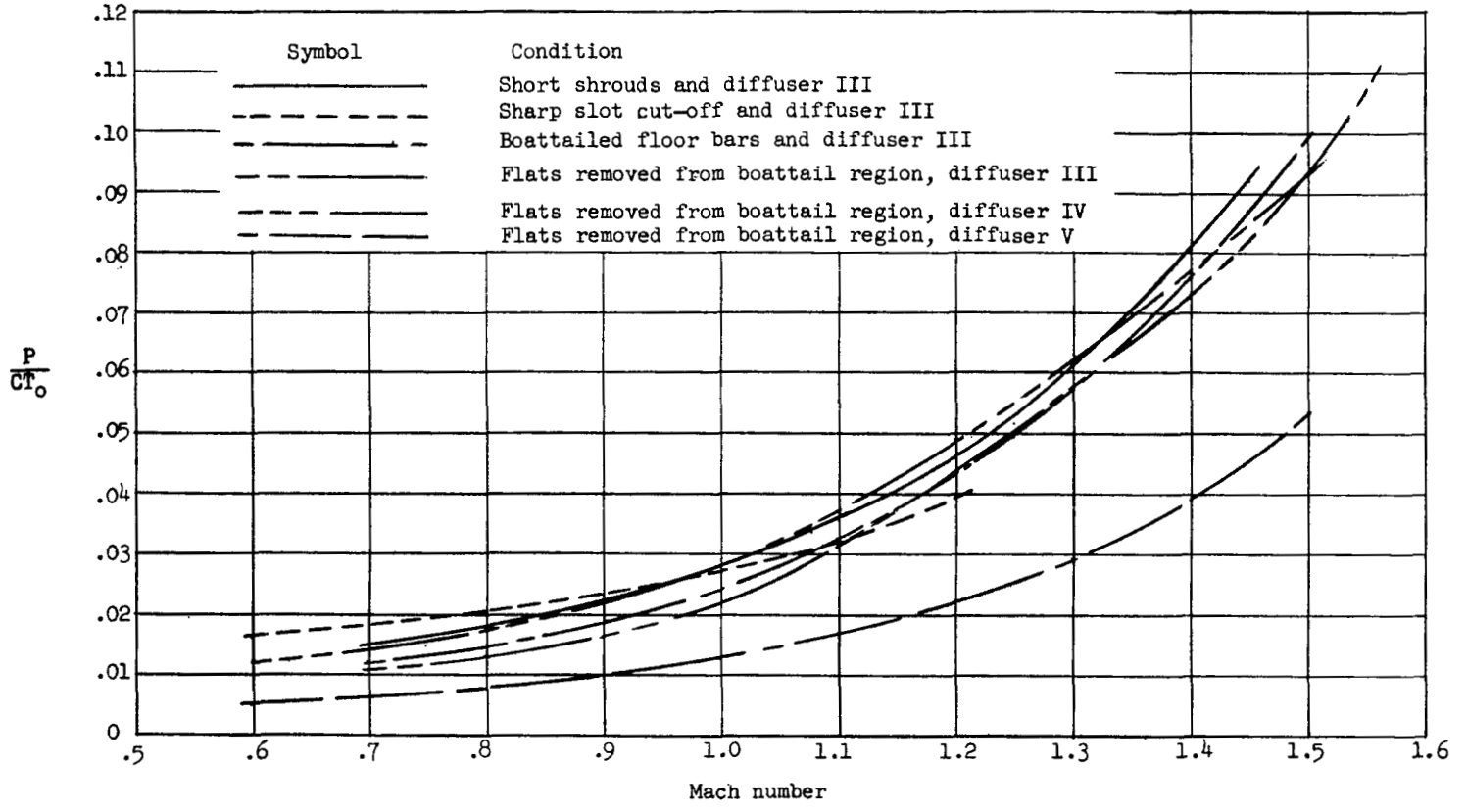

Figure 14.- Composite of the various envelope curves of the variation of power requirements with Mach number.